Zoologischer Anzeiger 291 (2021) 123–138

Contents lists available at ScienceDirect

Zoologischer Anzeiger

journal homepage: www.elsevier.com/locate/jcz

Research paper

Taxonomic status of *Apostolepis tertulianobeui* Lema, 2004 based on an integrative revision of *Apostolepis assimilis* (Reinhardt, 1861) (Serpentes: Dipsadidae)

Omar M. Entiauspe-Neto [a, *], Claudia Koch [b], Russell J. Gray [c], Arthur Tiutenko [d], Daniel Loebmann [e], Thaís B. Guedes [f]

[a] *Universidade Federal do Rio Grande, Instituto de Ciências Biológicas, Laboratório de Vertebrados, Av. Itália Km 8, CEP: 96203-900, Vila Carreiros, Rio Grande, Rio Grande do Sul, Brazil*
[b] *Zoologisches Forschungsmuseum Alexander Koenig, Adenauerallee 160, 53113, Bonn, Germany*
[c] *705 Alligator Ranch Rd. New Smyrna Beach, Florida, 32168, USA*
[d] *Friedrich-Alexander Universität Erlangen-Nürnberg, Schloßplatz 4, 91054, Erlangen, Germany*
[e] *Centro de Estudos Superiores de Caxias, Universidade Estadual do Maranhão, Praça Duque de Caxias, s/n, 65604-380, Caxias, MA, Brazil*
[f] *Gothenburg Global Biodiversity Center, Department of Biological and Environmental Sciences, University of Gothenburg, Box 461, SE-405 30, Göteborg, Sweden*

ARTICLE INFO

Article history:
Received 13 October 2020
Received in revised form
25 January 2021
Accepted 27 January 2021
Available online 8 February 2021

Corresponding editor: Dr. Alexander Kupfer

Keywords:
Cranial morphology
Elapomorphini
Hemipenial morphology
Neotropics
Species distribution modelling
Taxonomy

ABSTRACT

Apostolepis is a diverse Dipsadid snake genus, with 35 known species, inhabiting most of South America at east of the Andes. In this study, we redescribe *Apostolepis assimilis* Reinhardt, 1861, and evaluate the taxonomic status of a controversial taxon, *Apostolepis tertulianobeui*, described based on a single specimen from an unknown locality of Minas Gerais state, southeastern Brazil. A careful reanalysis of the type specimen and additional material provides compelling evidence for the synonymy of *A. tertulianobeui* with *A. assimilis*. We also provide comments on the taxonomy of *Apostolepis*, osteological and hemipenial descriptions, and a species distribution modelling for *A. assimilis*.

1. Introduction

Apostolepis Cope, 1887 is a neotropical Dipsadid genus, encompassing small to medium-sized snakes, with semi-fossorial or cryptozoic habits (Lema, 2001; Guedes et al., 2018; Entiauspe-Neto et al., 2019). This genus is widely distributed in most of South America east of the Andes, from south-western Colombia and the Guiana shield to southern Brazil and northwestern Argentina, from sea level up to 1,500 m of elevation, in almost all Neotropical biomes (Nogueira et al., 2019; Entiauspe-Neto et al., 2020a). *Apostolepis* is the most diverse Elapomorphini Jan, 1862 genus, with 35 known species (Entiauspe-Neto et al., 2019; 2020b; Uetz & Hošek, 2020).

The taxonomy of *Apostolepis* has been complicated and controversial; despite recent efforts in redescribing species and reports of new populations (e.g. Nogueira et al., 2012; Entiauspe-Neto et al., 2014, 2020a, b; Fermiano et al., 2020), several species remain known only from small series, and little is known regarding their morphological variation. Moreover, many descriptions are also based upon unreliable and variable characters, which has caused severe taxonomic instability in the genus (see Entiauspe-Neto et al., 2019; 2020a). We also consider *Parapostolepis polylepis* (Amaral, 1922 [1921]) as a valid combination, since the proposed synonymy of Ferrarezzi (1993) was never formally published; this species

* Corresponding author.
E-mail addresses: omarentiauspe@hotmail.com (O.M. Entiauspe-Neto), C.Koch@leibniz-zfmk.de (C. Koch), rgrayherpetology@gmail.com (R.J. Gray), arthur@tiutenko.de (A. Tiutenko), pinguimfiel@yahoo.com.br (D. Loebmann), thaisbguedes@yahoo.com.br (T.B. Guedes).

https://doi.org/10.1016/j.jcz.2021.01.004
0044-5231/

can be diagnosed from all other *Apostolepis* by having 17 dorsal rows without reduction, and was therefore omitted from this work.

Apostolepis assimilis (Reinhardt, 1861) is a medium-sized snake that is mainly distributed in open areas of Cerrado and adjacent regions in western Argentina, central-western, southern, southeastern, northwestern Brazil, and eastern Paraguay (Nogueira et al., 2019). The species was described by Reinhardt (1861) as *Elapomorphus assimilis*, based on a female specimen from Capão dos Porcos, Brumadinho municipality, Minas Gerais, southeastern Brazil. Although locally common, there is little available information on its morphological variation and taxonomic affinities.

Apostolepis tertulianobeui Lema, 2004a,b,c was described based on a juvenile male (MCN 8535) from "hinterland Minas Gerais", an unknown locality in Minas Gerais state, southeastern Brazil. The description of Lema (2004a,b,c) is particularly brief, relying exclusively upon external morphology, compared only against its sympatric congener, *Apostolepis assimilis* Reinhardt, 1861, based on the snout shape, head width, frontal plate size, shape of the tail and coloration. Ferrarezzi et al. (2005) proposed the synonymy of *A. tertulianobeui* with *A. assimilis*, although without examining the holotypes of both species. Upon examining a large series of *A. assimilis*, Lema & Renner (2007) revalidated *A. tertulianobeui*, based on significant differences in coloration between the species. Later, Lema & Renner (2012) described *Apostolepis parassimilis*, based on a holotype (MCN 8535, juvenile male) from Uberlândia, Minas Gerais state, southeastern Brazil, and a paratype (MNRJ 6524, juvenile female) from "Bahia", northeastern Brazil. Costa & Bérnils (2015) noticed that *A. tertulianobeui* and *A. parassimilis* shared the same holotype, and considered both as objective synonyms, giving priority to *A. tertulianobeui*. Nogueira et al. (2019) reported new specimens of *A. tertulianobeui* and affixed its type locality as "Uberlândia", in Minas Gerais, southeastern Brazil.

In this work, we re-examine the type series of both species, and reevaluate their taxonomic status. We also provide a redescription for *A. assimilis* based on the discovery of new specimens, a species distribution modeling, osteological and hemipenial description, and comments on the taxonomy of the group.

2. Material and methods

2.1. Morphological analyses

We examined 648 specimens of *Apostolepis* from the following collections: Academy of Natural Sciences, USA (ANSP); The Natural History Museum, UK (NHM, previously BMNH); Coleção Herpetológica Universidade Federal do Rio Grande, Brazil (CHFURG); Coleção Herpetológica da Universidade Federal do Ceará, Brazil (CHUFC); Coleção Herpetológica da Universidade Federal de Sergipe, Brazil (CHUFS); Instituto Butantan, Brazil (IBSP); Instituto de Ciencias Naturales, Universidad Nacional de Colombia, Colombia (ICN); Coleção Herpetológica, Instituto de Pesquisas Amazônicas, Brazil (INPA); Museu de Ciências e Tecnologia da Pontifícia Universidade Católica do Rio Grande do Sul, Brazil (MCP); Muséum National d'Histoire Naturelle, France (MNHN); Museo de Historia Natural Para la Tierra, Paraguay (MHNP); Museu Nacional, Brazil (MNRJ); Museu de História Natural da Universidade Federal de Alagoas, Brazil (MUFAL); Museu de Zoologia, Universidade Estadual de Feira de Santana, Brazil (MZUEFS); Museu de Zoologia da Universidade Federal da Bahia, Brazil (MZUFBA); Museu de Zoologia da Universidade de São Paulo, Brazil (MZUSP); Naturhistorisches Museum Wien, Austria (NHMW); Senckenberg Natural History Museum, Germany (SMF); Coleção Herpetológica da Universidade Federal do Mato Grosso, Brazil (UFMT); Coleção Herpetológica da Universidade Federal de Rondônia, Brazil (UFRO-H); University of Michigan Museum of Zoology, Herpetology collection, USA (UMMZ); Zoologisches Forschungsmuseum Alexander Koenig, Germany (ZFMK); Zoologisches Museum für Naturkunde Berlin, Germany (ZMB). A list of examined material is provided in Appendix 1.

Scale counts follows Dowling (1951). Sex was determined by a ventral incision in the base of the tail. An emended diagnosis is based on the nomenclature used by Entiauspe-Neto et al. (2020a). Morphometric characters are as follows: head length (HL), measured from center of rostral to the corner of the mouth; head width, measured at the corner of mouth; snout-vent length (SVL), ventrally measured from rostral to the posterior margin of cloacal scale; tail length (TL), measured from posterior margin of cloacal scale to terminal scale. Head and tail measurements were taken with a dial caliper to the nearest 0.01 mm; for others, a flexible ruler was used. Scales were measured on the right side of head. We prepared hemipenes following procedures of Pesantes (1994) for retracted or semi-everted organs from preserved specimens. Calcified structures were colored with red dye Alizarine S. Hemipenial morphology terminology follows Dowling & Savage (1960), Zaher (1999), and Zaher & Prudente (2003). Species concepts follow De Queiroz (2007). Taxonomically valid *Apostolepis* species follow Entiauspe-Neto et al. (2019) and Entiauspe-Neto et al. (2020a,b,c).

Osteological description of the skull of a specimen of *A. assimilis* (ZFMK 102120) is based on a high-resolution micro-CT scan, performed with a Bruker SkyScan 1173 at ZFMK. The scan used an X-ray beam with 43 kV source voltage and 114 μA current without filters. Rotation steps of 0.3° were used with a frame averaging of 3, recorded over a 180° rotation, resulting in 800 projections of 500 ms exposure time each and a total scan duration of 33 min 49 s. The magnification setup generated data with an isotropic voxel size of 8.16 μm. The CT-dataset was reconstructed using N-Recon software version 1.7.1.6 (Bruker MicroCT) and rendered in three dimensions through the aid of Amira visualization software (FEI, Thermo Fisher Scientific). Segmentation to separate and color the bones was also performed using Amira. Osteological terminology follows Bullock & Tanner (1966) and Cundall & Irish (2008), and the description of the skull follows Entiauspe-Neto (2020). We compared our osteological description with data available for *Apostolepis* from Entiauspe-Neto et al., (2020), Ferrarezzi et al. (2005), and McDowell (1986).

2.2. Statistical analyses

Because some Apostolepis species are known to exhibit sexual dimorphism in meristic counts and morphometric characters (e.g. Braz et al., 2019), we employed a series of independent Mann–Whitney U tests to test for sexual dimorphism. We used a non-parametric test because our small sample size violated assumptions of univariate normality and homoscedasticity, which were evaluated Kolgomorov-Smirnov and Levene's tests, respectively (Zar, 1999). The evaluated morphometric variables were: snout-vent length (SVL), tail length (TL), tail-to-body ratio (TL/(SVL + TL) * 100). The evaluated meristic variables were: ventral scale counts and subcaudal scale counts. The assumption of the null hypothesis was that both sexes have equal morphometric measurements, therefore rejection of the null hypothesis ($p \leq 0.05$) indicate significant variation between males and females.

2.3. Species distribution modelling

To model the distribution of *A. assimilis*, we used the MaxEnt algorithm via the r package dismo (Hijmans et al., 2017), and evaluated model performance using functionality of the ENMeval (Muscarella et al., 2016) and rmaxent (Baumgartner et al., 2017)

packages. Visualizations were made using the packages ggplot2 (Wickham, 2011) for basic graph parameters, raster (Hijmans et al., 2015) for classes and functions to manipulate geographic (spatial) data in 'raster' format, and rasterVis (Lamigueiro et al., 2019) for the use of methods for enhanced visualization and interaction with raster data. Occurrence data (N = 709) was retrieved from Nogueira et al. (2019), which were collated from 1861 to 2019. Records with non-applicable values, duplicate values, anomalous values, and incomplete values (i.e. coordinates with only 2 decimal place values) were removed. Occurrence data used in the model included 354 confirmed records. The model was separated into testing and training data based on a 5-block partition k-fold cross-validation method, expanding on concepts from Radosavljevic & Anderson (2014), where k 1–4 partitions were used as training data and the k 1 partition was used as testing data. Response variables retrieved for the models included bioclimatic variables (Fick & Hijmans 2017), elevation, mean temperature (aggregated into annual mean), and precipitation (aggregated into annual mean). Variables were checked for multicollinearity and correlation issues via the usdm package (Naimi, 2015) functions vifstep with a threshold set to 10, and vifcor with a threshold set to 0.7. Since temperature, precipitation, and Human Influence variables have been reported to be some of the most important variables for reptile distribution models (Bradie & Leung, 2017), they were maintained in the final set of variables regardless of correlation issues. However, after running preliminary models it was found that the Human Influence Index (Sanderson et al., 2002) caused significant underfitting errors, so it was also removed. It is worth noting, however, that unlike ensemble models and other algorithms, MaxEnt accounts for redundant variables and is robust to predictor collinearity in model training (Feng et al., 2019). After several runs of the model, other variables were dropped due to a lack of variable/permutated importance and response significance. The remaining response variables included after optimization of the final model were: Bio2, Bio3, Bio9, Bio15, Bio18, elev, mean annual temperature, and mean annual precipitation (Table 1). Before running the final model, values were extracted from the response variables to determine mean and standard deviation of observed locations to ensure output responses were sensible. Finally, response variables and predicted model outputs were cropped to a single tile layer (xmin/max = −60, −30; ymin/max = −30, 0) a total area of extending from the mean latitude and longitude of the occurrence records as an absence mask. Since geographic range data of snakes in this region of South America have been extensively surveyed and collected (Nogueira et al., 2019), we considered the predicted area outside of this large range to be unlikely. The final model was evaluated using geographically constrained random points (N = 1000) across all variables and validated by measure of AUC. All model parameterization and output reporting were based on standardized protocols outlined by Zurell et al. (2020).

3. Results

3.1. Identity of Apostolepis tertulianobeui

The holotype of *A. tertulianobeui* (MCN 8535, Fig. 1, top) is identified as a "young male", by Lema (2004a,b,c). Overall inspection of the individual reveals two semi-everted hemipenes and an SVL of 360 mm; we consider it to be an adult male. It is diagnosed exclusively against *A. assimilis* (characters in parenthesis), for which it is said to differ based on "*slender and projecting snout (broad and not projecting), head larger than neck posteriorly (head equal to neck), very small frontal plate (relatively large frontal plate), end of tail slightly compressed (conical), restricted black head cap (extensive), black tail blotch only dorsal (complete), and terminal shield white (black)*" (Lema, 2004a,b,c:156). The author also provides a comparative table among *A. tertulianobeui*, *A. assimilis*, and *A. flavotorquata*, comparing characters of "*Head x neck; Head height; Snout projecting; Snout tip; Jaws anterior margin; Orbit x distance to oral margin; Tail end; Terminal plate; Mental region; Black tail blotch; Terminal*" (Lema, 2004a,b,c:158).

Fig. 1. Overview of *Apostolepis assimilis* (ZMUC 63806, bottom) and *A. tertulianobeui* (MCN 8535, top) holotypes. Scale bar = 10 mm. Photo credits: P. R. Møller (bottom), R. Oliveira (top). Figure should be grayscale in print.

Regarding snout morphology, our examination of the holotype (Figs. 1 and 2) reveals a short, broad, and slightly projecting snout. The head illustration of *A. tertulianobeui*, provided by Costa & Bérnils (2015:244) shows the aforementioned characters. A "slender and projecting snout" is present in other *Apostolepis* species, such as *Apostolepis dimidiata* (Jan, 1862) and *Apostolepis intermedia* (Koslowsky, 1898), in which the rostral projects greatly over the inferior maxilla and symphisal; it is not the case for the holotype of *A. tertulianobeui*.

The second mentioned diagnostic character, head size proportion, is also incorrectly described by Lema (2004a,b,c). The holotype head is indistinct from the body, corresponding to the diagnosis of *A. assimilis* as proposed by Lema (2004a,b,c). However, we note that this diagnostic character is highly variable and should be dismissed; Cruz-da-Silva et al. (2018) presents head photographs for two specimens of *A. assimilis*, in which the heads are larger than the

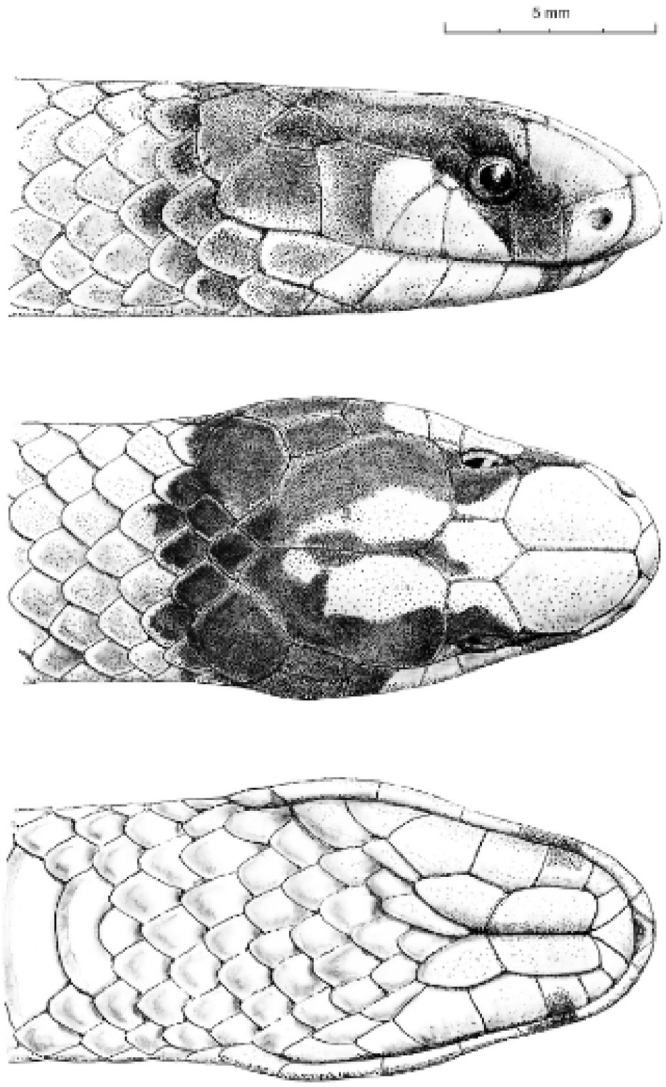

Fig. 2. Head view of *Apostolepis tertulianobeui* (MCN 8535, holotype). Figure should be grayscale in print.

body width. Although this character was not carefully evaluated in our sample, we note that it is not taxonomically relevant, because it is prone to individual variation.

The third mentioned character is a "very small frontal plate". The author did not provide exact measurements, therefore it is impossible to compare it. The fourth character, "end of tail slightly compressed" in *A. tertulianobeui*, versus "conical" in *A. assimilis* also could not be clearly distinguished, as both tails are seemingly identical upon comparison of their shape. A "restricted black head cap" likely refers to the black dorsal coloration of the head from the holotype of *A. tertulianobeui*, which has a large white snout blotch, covering its rostral, nasals, prefrontals, frontal, supraoculars and parietals. We have encountered specimens of *A. assimilis* with degrees of variation for this character. It is also found to be variable within a single population of *A. assimilis* by Cruz-da-Silva et al. (2018), and considered polymorphic by Entiauspe-Neto et al. (2020a) for other *Apostolepis* species.

The last characters, the black tail blotch size and terminal scale color, are also imprecisely described by Lema (2004a,b,c). Our examination showed that its terminal scale is black dorsally and laterally, with white pigmentation on its ventral surface. The black tail blotch, said to be "only dorsal" by Lema (2004a,b,c), can also occur on the ventral surface of *A. tertulianobeui*, although faded to dark brown. A bicolor terminal scale may also be attributed to individual variation or fading coloration. All other characters of *A. tertulianobeui*, such as ventral scale counts, subcaudals, supralabials and infralabials, also fall within the reported range for *A. assimilis*. In light of this, we propose *A. tertulianobeui* should be relegated to a junior synonym of *A. assimilis*. Other specimens identified as *Apostolepis tertulianobeui* represented a conglomerate of taxa, namely *A. assimilis*, *A. cearensis*, and *A. sanctaeritae*.

3.2. Redescription of *Apostolepis assimilis*

Apostolepis assimilis (Reinhardt, 1861).
Elapomorphus assimilis Reinhardt, 1861:235.
Apostolepis tertulianobeui Lema, 2004a,b,c:156. **New synonymy**.
Apostolepis parassimilis Lema & Renner, 2011:73. **New synonymy**.

3.2.1. Holotype

Adult female (ZMUC 63806, holotype), from Capão dos Porcos, Brumadinho (20°08′34″ S, 44°12′0″ W, 718 m elevation), Minas Gerais state, Brazil.

3.2.2. Diagnosis

This species presents (1) dorsal scales 15/15/15; (2) preocular present, separated from nasal; (3) loreal absent; (4) temporals 0 + 1 (rarely 1 + 1 or 0 + 0); (5) supralabials six (rarely five or seven), 2nd–3rd in contact with orbit; (6) infralabials six or seven (rarely eight), 1st–4th in contact with anterior chinshields; (7) ventrals 230–268 (225–260 males, 243–267 females); (8) subcaudals 24–39 (28–39 males, 24–35 females); (9) dorsal pattern uniform red or orange (vertebral and dorsoventral stripes rarely present, vestigial); (10) ventral pattern uniform red, head and tail black (rarely, infralabials and chinshields white); (11) white nuchal collar covering 1–5 rows, black nuchal collar covering 1–4 rows; (12) caudal blotch 8–11 scales wide on dorsum, 7–11 in venter, terminal scale black (rarely white or bicolor); (13) supralabial blotch medium sized, covering two or three supralabial scales and postocular; (14) maxillary teeth 3 + 2 or 4 + 2; (15) SVL 140–780 mm, TL 10–55 mm.

Fig. 3. Colour pattern in life of *Apostolepis tertulianobeui* (MCN 8535, holotype, top) and *Apostolepis assimilis* (ZMUC 63806, holotype, bottom). Figure should be grayscale in print. (For interpretation of the references to colour in this figure legend, the reader is referred to the Web version of this article.)

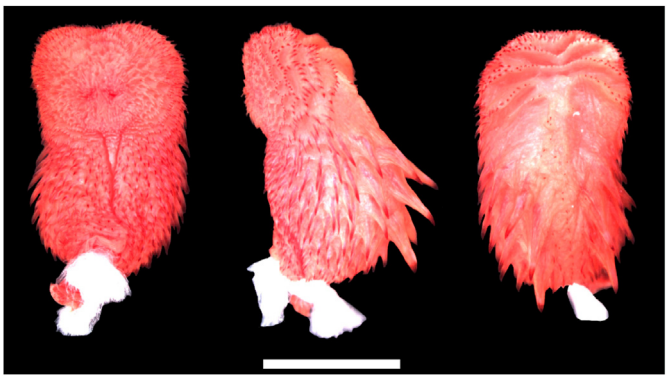

Fig. 4. Sulcate, lateral, and asulcate views of the *Apostolepis assimilis* (IB 52754) hemipenis. Scale bar = 10 mm. Figure should be grayscale in print.

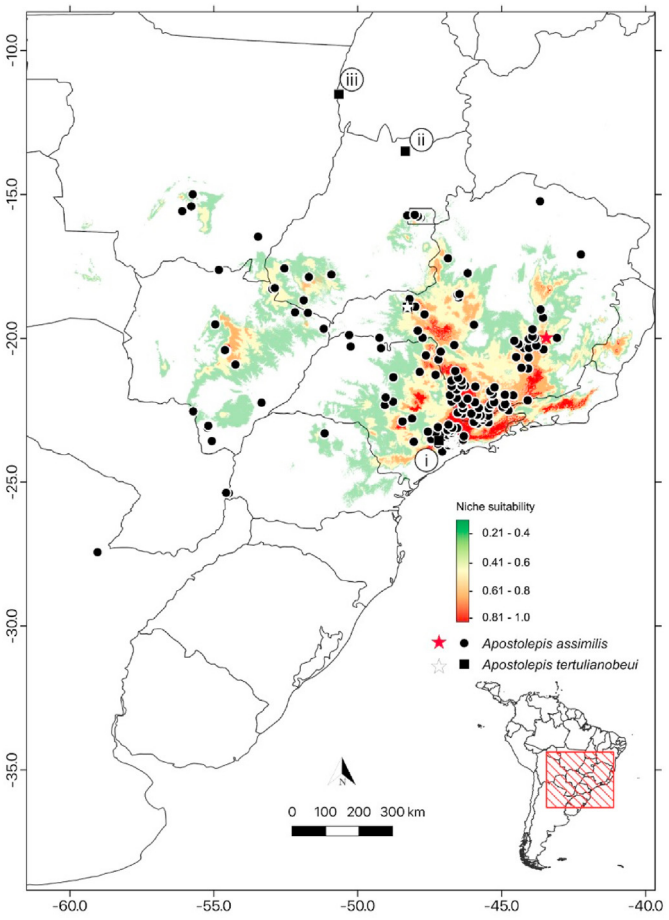

Fig. 5. Geographic distribution and species distribution model of *Apostolepis assimilis* and *Apostolepis tertulianobeui*. Stars = Type localities; Record I: reidentified as *A. assimilis*; Record II: reidentified as *A. assimilis*; Record III: reidentified as *A. sanctaeritae*. Figure should be grayscale in print.

3.2.3. Comparisons

Apostolepis assimilis can be misidentified with other three red *Apostolepis* that occur in the Cerrado: *Apostolepis cearensis* Gomes, 1915, *Apostolepis flavotorquata* (Duméril, Bibrón, and Duméril, 1854), and *Apostolepis sanctaeritae* Werner, 1924. Data from other species will be presented inside parenthesis. The first species, *A. cearensis* (Fig. 6, E), can be diagnosed from *A. assimilis* based on its light supralabial blotch relatively larger size (small or indistinct, usually restricted to 4th supralabial), white nuchal collar reaching up to 1–5 rows (4–5 rows long), white ventral head coloration (usually black), smaller range of ventrals, 225–260 males, 243–267 females (215–237 males, 227–248 females), smaller and usually single shaped rostral blotch (usually divided and not reaching up to the frontal scale), white rostral blotch (orange), and acuminate snout shape (projected) (Ferrarezzi et al., 2005).

Apostolepis flavotorquata (Fig. 6, G) can be diagnosed from *A. assimilis* based on its distinct white ventral coloration in life (yellow), smaller and distinctly shaped rostral white blotch (divided and not reaching up to the frontal scale), black nuchal collar covering 1–4 rows (up to two scales wide), usually undivided light supralabial blotch (divided, covering four supralabials), hemipenis small and slightly bilobed (organ long and simple, spinules restricted to proximal area, enlarged spines absent, asulcate surface calyculate) (Lema & Renner, 2005).

Apostolepis sanctaeritae (Fig. 6, F) can be readily diagnosed from *A. assimilis* by having an additional white nuchal collar; however, this nuchal collar might not be visible in preserved specimens, but other characters can be verified, as *A. assimilis* will have a black nuchal collar covering 1–4 rows (4–7 scales wide), relatively larger light supralabial blotch (small or indistinct, usually restricted to 4th supralabial), white snout blotch coloration in life (orange), hemipenial morphology with smaller spines on asulcate side (larger spines on asulcate side) (Guedes et al., 2018a; Entiauspe-Neto et al., 2020b).

From *Apostolepis albicollaris* Lema, 2004a,b,c (Fig. 6, H), it can be distinguished based on its uniformly red dorsal pattern (two lateral black stripes), an entire snout blotch (divided), and a smaller (up to three scales) white supralabial blotch (up to five scales wide).

An extralimital species, *Apostolepis quirogai* Giraudo & Scrocchi 1998 (Fig. 6, J), presents a similar coloration pattern, nuchal collar, tail and snout blotch; it can be distinguished from *A. assimilis* based on its uniformly red dorsal pattern (two lateral black stripes).

Two other extralimital species, *Apostolepis multicincta* Harvey, 1999 (Fig. 6, I) and *Apostolepis dorbignyi* (Schlegel, 1837) are remarkably similar to *A. assimilis*. Although we have encountered great difficulty in distinguishing *A. multicincta* from *A. dorbignyi*, as they are sympatric and have a near total overlap of their diagnostic features, until their taxonomic status is evaluated, we can distinguish them from *A. assimilis* based on their tail tip coloration (white), black in the former species.

Furthermore, *A. assimilis* can be distinguished from *Apostolepis adhara* França, Barbo, Silva-Jr, Silva, and Zaher, 2018, *Apostolepis arenaria* Rodrigues, 1993, *Apostolepis borelli* Peracca, 1904, *Apostolepis breviceps* Harvey, Gonzales, and Scrocchi, 2001, *Apostolepis cerradoensis* Lema, 2003, *Apostolepis christineae* Lema, 2002, *Apostolepis dimidiata* (Jan, 1862), *Apostolepis gaboi* Rodrigues, 1993, *Apostolepis goiasensis* Prado, 1942, *Apostolepis intermedia* Koslowsky, 1898, *Apostolepis kikoi* Santos, Entiauspe-Neto, Araújo, Souza, Lema, Strüssmann, and Albuquerque, 2018, *Apostolepis lineata* Cope, 1887, *Apostolepis longicaudata* Gomes, 1915, *Apostolepis nelsonjorgei* Lema & Renner, 2004, *Apostolepis niceforoi* Amaral, 1935, *Apostolepis nigrolineata* (Peters, 1869), *Apostolepis nigroterminata* Boulenger, 1896, *Apostolepis phillipsi* Harvey, 1999, *Apostolepis quirogai* Giraudo & Scrocchi, 1998, *Apostolepis serrana* Lema & Renner, 2006, *Apostolepis striata* Lema, 2004a,b,c, *Apostolepis tenuis* Ruthven, 1927, *Apostolepis thalesdelemai* Borges-Nojosa, Lima, Bezerra, and James, 2017, *Apostolepis underwoodi* Lema & Campbell, 2017, and *Apostolepis vittata* (Cope, 1887) based on a combination of its uniformly red dorsal pattern (none, two, three, five, seven, or eleven dorsal stripes, over red, yellow, brown, black or gray background coloration) with presence of white and black


A
B
C
D
E
F
G
H
I
J

nuchal collars (nuchal collars absent in *A. breviceps*, *A. christineae*, *A. dimidiata*, *A. goiasensis*, *A. intermedia*, *A. lineata*, *A. longicaudata*, *A. niceforoi*, *A. serrana*, *A. striata*, *A. vittata*, variable for *A. nigrolineata* and *A. thalesdelemai*). Although *Apostolepis ambiniger* (Peters, 1869) bears a uniformly red dorsal pattern, it can be distinguished from *A. assimilis* in lacking nuchal collars.

3.2.4. Redescription

Head rounded in dorsal view, arched in lateral view; cervical constriction absent; snout rounded in dorsal view, slightly projecting in lateral view; nasal as long as wide, in contact with rostral, first two supralabials and prefrontals; prefrontals paired, as long as wide, in contact with rostral, nasal, supraocular, frontal and preocular; supraocular as long as wide; frontal hexagonal, longer than wide; internasals absent; loreal absent; preocular present, separated from nasal; eye medium; postocular single (rarely paired or absent), longer than wide; temporals 0 + 1 (rarely 1 + 1 or 0 + 0); occipitals on both sides of head, single or paired, contacting parietal, anterior temporal (when present) and sixth supralabial; supralabials six (rarely five or seven), first in contact with nasal and rostral, second in contact with prefrontal and preocular, 2–3 in contact with orbit, fourth in contact with postocular, fifth in contact with parietal and temporal, sixth in contact with occipital and temporal; infralabials six or seven (rarely eight), first pair in contact with mental and anterior chinshields, second and third pair in contact with anterior chinshields, pairs 4–6 in contact with posterior chinshields and gulars; maxillary teeth 3 + 2 or 4 + 2; tail short.

3.2.5. Coloration in life

Head dorsally black, with white rostral blotch single (rarely divided), covering prefrontals, rostral, and external edge of frontal and supraoculars (rarely, in reduced form, covering only prefrontals and rostral, or in elongated form, covering frontal, supraoculars and parietals); lateral portion of head black, white supralabial blotch small, covering two or three supralabials and postocular; ventral portion of head black, with white pigmentation on infralabials, chinshields, symphisal and gulars; dorsum uniformly orange or red (vertebral and lateral stripes rarely present, vestigial); ventral coloration uniform orange or red; white nuchal collar covering 1–5 dorsal rows, black nuchal collar covering 1–4 dorsal rows; caudal blotch 8–11 scales wide on dorsum, 7–11 in venter, terminal scale black (rarely white or bicolor).

3.2.6. Coloration in preservative

Black coloration becomes brown; orange and red coloration becomes white. The white nuchal collar may faded and be indistinct from body coloration.

3.2.7. Meristic and morphometric variation

Apostolepis assimilis exhibited significant sexual dimorphism in ventral ($U_{43} = 44$, $p < 0.001$) and subcaudal ($U_{38} = 45$, $p < 0.001$) scale counts, as well as SVL ($U_{27} = 130$, $p = 0.05$), and tail-to-body ratio ($U_{24} = 30$, $p = 0.02$), although not for tail length itself ($U_{24} = 48$, $p = 0.2$).

SVL in males 140–540 mm (313 ± 123.6; $n = 12$), in females 210–780 mm (420.4 ± 141.4; $n = 15$). TL in males 11–55 mm (34.9 ± 12.8; $n = 11$), in females 10–50 mm (28.5 ± 10.1; $n = 13$). Ventral scales in males 225–260 (239 ± 8.9; $n = 21$), in females 243–268 (254 ± 7.8; $n = 22$). Subcaudal scales in males 26–36 (31 ± 2.7; $n = 19$), in females 24–31 (27 ± 2; $n = 19$).

3.2.8. Hemipenis

Hemipenis slightly bilobed, noncapitate, semicalyculate (Fig. 4); lobes poorly differentiated, present strictly on distal portion of capitulum; lobes slightly clavate, tips rounded, with spinules centrifugally oriented from its medial surface; lobes and capitulum uniformly covered with papillate calyces on sulcate side; lateral portion of capitulum with calyculate flounces; capitulum present only on sulcate side; capitulum slightly above *sulcus spermaticus* bifurcation, which is on the middle of organ; capitulum slightly smaller than hemipenial body; capitular groove slightly distinct on both sides; *sulcus spermaticus* branches centrolineally oriented, becoming indistinct to capitulum; margins of *sulcus spermaticus* thin, entirely adjacent to spinules; hemipenial body subcylindrical; on sulcate side, hemipenial body covered by moderately sized hooked spines; on asulcate side, hemipenial body with a basal naked pocket extended to medial region, followed by transversely oriented papillate flounces; two to three rows of enlarged spines present on lateral portion of sulcate side and medial region of asulcate side (Fig. 4).

3.2.9. Geographic distribution

Widely distributed in Brazil (Distrito Federal, Goiás, Mato Grosso, Mato Grosso do Sul, Minas Gerais, Paraná, São Paulo), western Paraguay (Canindeyu, Alto Parana), and northwestern Argentina (Misiones), with unconfirmed or erroneous records for some states in Brazil (Rondônia, Santa Catarina, Rio Grande do Sul) (Fig. 5). Occurs in open areas of Cerrado and adjacent regions (Pantanal, Atlantic Forest) (Nogueira et al., 2019). Its distribution in the Caatinga is restricted to northern Minas Gerais state. A specimen reported from Tanque do Aragão, Bahia (MNRJ 6524), is actually a misidentified *A. cearensis*. A specimen reported from Fortín Toledo, Boquerón, Paraguay by Smith & Clay (2015) is clearly a *Tantilla melanocephala* (Linnaeus, 1758). A specimen from Jacaré, Alto Xingu, Mato Grosso (SMS 93352) is a misidentified *A. flavotorquata*. Records of Nogueira et al. (2019) from Tocantins (e.g. IBSP 12324) refer to *A. sanctaeritae*. Our examined record from Santa Catarina (ZFMK 102210, previously BGSS5344) is possibly in error, as it likely represents a shipping locality. We consider the occurrence of this species for Rondônia and Rio Grande do Sul states as unlikely, and no vouchers were encountered for these states.

3.2.10. Species distribution modelling

Response variables used in the species distribution model showed varying influence and importance for *Apostolepis assimilis*; these are presented as supplemental material (Supp. Fig 1). See Table 1 for description of response variables used. Observed values for elevation (809.21 m ± 236.62 m) were shown to be the most influential of the model covariates, followed by precipitation of the warmest quarter (604.77 mm ± 102.92 mm), Bio15 (65.53% ± 11.73%), mean precipitation (121.37 mm ± 11.36 mm), annual mean diurnal range (11.50 °C ± 1.07 °C), mean temperature

Fig. 6. Red *Apostolepis* specimens from the Atlantic Forest, Chaco, Cerrado, and Caatinga in life. A: *Apostolepis assimilis* from Brasília, Federal District, Brazil (CHUNB, without voucher); B–D: *Apostolepis assimilis* from São Paulo, Brazil (IBSP, without voucher); E: *Apostolepis cearensis* from Mucugê, Bahia, Brazil (unvouchered); F: *Apostolepis sanctaeritae* from the Jalapão region, Tocantins, Brazil; G: *Apostolepis flavotorquata* from Estreito, Maranhão, Brazil; H: *Apostolepis albicollaris* from Brasília, Distrito Federal, Brazil; I: *Apostolepis multicincta* from Santa Cruz, Bolivia; J: *Apostolepis quirogai* from Misiones, Argentina. Photo credits: L. J. Vitt (A, F), W. Wüster (B), TBG (C), M. A. Freitas (E), C. Cintra (F), G. Horta (G), A. D. Abegg (D), S. Reichle (I), and A. Martínez (J). Figure should be grayscale in print. (For interpretation of the references to colour in this figure legend, the reader is referred to the Web version of this article.)

Table 1
Response variables used in the final SDM with units of measurement and interpretations. Bioclimatic variable interpretations are based on the USGS guide by O'Donnell et al. (2012).

Response Variable	Interpretation
Bio2	Annual mean diurnal range (°C): provides information on the relevance of temperature fluctuation
Bio3	Isothermality (%): useful for tropical, insular and maritime environments; informs on the relevance of day-to-night and summer-to-winter oscillations
Bio9	Mean temperature of the driest quarter (°C): useful in examining relevance on seasonal distributions during the driest three months of a year
Bio15	Precipitation seasonality (%): represents precipitation variability; larger percentages suggest greater variability and smaller percentages suggest static annual precipitation
Bio18	Precipitation of the warmest quarter (mm): Total precipitation of the warmest three months which may affect seasonal distributions
Elevation	Vertical distance from geographic area above sea level (m)
Mean temp.	Mean annual temperature (°C)
Mean prec.	Mean annual precipitation (mm)

(19.88 °C ± 2.15 °C), and isothermality (64.14% ± 3.99%). Variable contribution represents the environmental variables which contribute to the fitted model during training, while variable importance reflects the contributions of a given variable trained on the final MaxEnt model (Phillips, 2006).

The final modelled distribution proved to have high accuracy (AUC = 0.96), while exhibiting sensible distribution area estimates based on response variables (Fig. 5). Probability of distribution slightly decreased with increasing diurnal range temperature fluctuations (annual mean diurnal temperature range), while remaining relatively static with isothermality (isothermality). A steep decrease in distribution probability occurred with increasing seasonal dryness (mean temperature of the driest quarter), while only light, insignificant fluctuations were shown for changes in precipitation seasonality (precipitation seasonality). Probability of distribution increased with the increase of precipitation during the warmest quarter (precipitation of the warmest quarter), and sharply increased with increasing elevation. Little to no response in distribution probability was shown for changes in mean annual temperature and humidity.

For a general potential distribution area estimate for *A. assimilis*, the predicted distribution was split into two polygons: 1) predicted distribution >0.05 (overall distribution), and 2) predicted area >0.5 (core distribution). The overall distribution covered an area of approximately 1,331,169 km^2, the majority of the potential distribution occurring throughout southern Brazil, with outer fragments in the northeastern regions of Paraguay and the eastern regions of Bolivia. The core distribution spanned over an area of approximately 241,109 km^2 and occurred almost exclusively in southern Brazil with small visible fragments of suitable areas in eastern Bolivia.

Apostolepis assimilis is widely distributed throughout southern Brazil with small populations in northeastern Paraguay and eastern Bolivia. The most influential factor for its distribution was elevation in which the probability of occurrence sharply increases with increasing el up to ~2000m above sea level. Another influential factor is mean temperature of the driest quarter (Bio9), in which probability of occurrence sharply decreased as temperatures increased, while also sharply increasing during the precipitation of the warmest quarter (Bio18). This inverse relationship between temperatures and precipitation seasonality may be explained by seasonal distributions of the species during periods of drought and torrential rain. Finally, annual mean diurnal temperature range (Bio2) had a somewhat influential contribution to distribution probability, which decreased as temperatures increased. Since the annual mean diurnal temperature range variable is indicative of temperature fluctuations in a given space, this may explain that *A. assimilis* prefers relatively static environmental conditions.

3.2.11. Osteology

Description based on an adult individual (ZFMK 102120; Figs. 7–9). Snout complex is composed of the premaxillae, nasals,

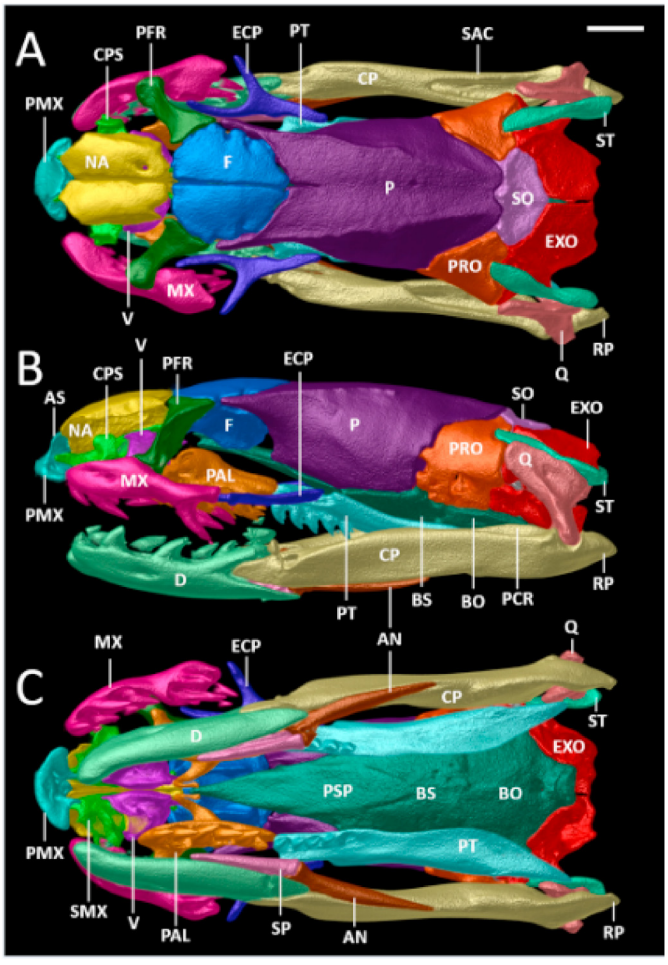

Fig. 7. Micro-CT images of the skull of *Apostolepis assimilis* (ZFMK 102120) in A) dorsal, B) lateral, and C) ventral views; AN (angular); AS (ascending process of premaxilla); BO (basioccipital); BS (basisphenoid); CP (compound bone); CPS (conchal process of septomaxilla); D (dentary); ECP (ectopterygoid); EXO (exoccipital); F (frontal); MX (maxilla); NA (nasal); P (parietal); PAL (palatine); PCR (prearticular crest of compound bone); PFR (prefrontal); PMX (premaxilla); PRO (prootic); PSP (parasphenoid rostrum); PT (pterygoid); Q (quadrate); RP (retroarticular process of compound bone); SAC (surangular crest of compound bone); SMX (septomaxilla); SO (supraoccipital); SP (splenial); ST (supratemporal); V (vomer). Scale bar = 1 mm. Figure should be gray-scale in print.

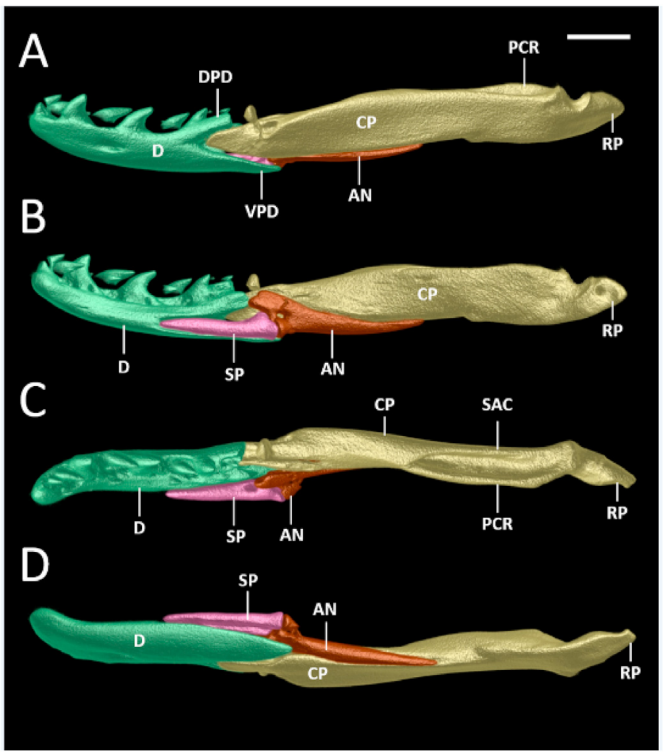

Fig. 8. Micro-CT images of the mandibula of *Apostolepis assimilis* (ZFMK 102120) in A) lateral, B) medial, C) dorsal, and D) views; AN (angular); CP (compound bone); D (dentary); DPD (dorsal process of dentary); PCR (prearticular crest of compound bone); RP (retroarticular process of compound bone); SAC (surangular crest of compound bone); SP (splenial); VPD (ventral process of dentary). Scale bar = 1 mm. Figure should be grayscale in print.

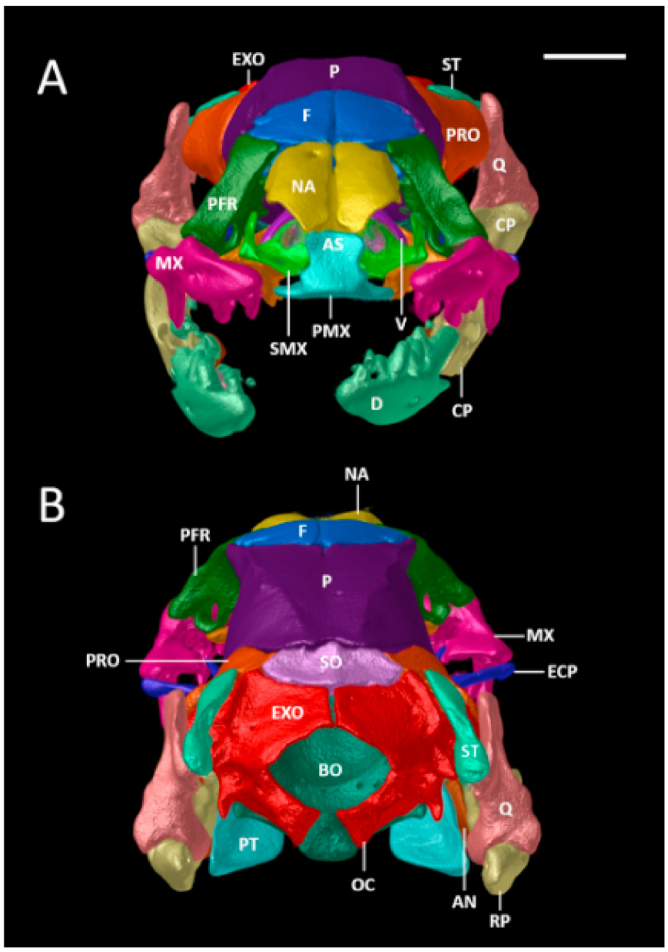

Fig. 9. Micro-CT images of the skull of *Apostolepis assimilis* (ZFMK 102120) in A) anterior, and B) posterior views; AN (angular); AS (ascending process of premaxilla); BO (basioccipital); CP (compound bone); D (dentary); ECP (ectopterygoid); EXO (exoccipital); F (frontal); MX (maxilla); NA (nasal); OC (occipital condyle); P (parietal); PFR (prefrontal); PMX (premaxilla); PRO (prootic); PT (pterygoid); Q (quadrate); RP (retroarticular process of compound bone); SMX (septomaxilla); SO (supraoccipital); ST (supratemporal); V (vomer). Scale bar = 1 mm. Figure should be grayscale in print.

septomaxillae, vomers, and prefrontals. The single premaxilla is edentulous, thick and robust, 1.8 times broader than high, with a stout, posterodorsally oriented ascending process, almost rectangular, but with a notch on each side on half height, slightly concave and posterodorsally contacting anterior end of nasals; lateral processes visible in dorsal view, moderately long, together making up half the width of the premaxilla, approaching but still distinctly separated from maxillae; vomerine processes posteriorly oriented, triangular, with a sharp point, that dorsally contacts the anteroventral part of body of the septomaxilla, largely separated from anterior end of vomers; ventral surface of premaxilla pierced by four foramina.

The paired nasals are roughly rectangular in dorsal view, about three times longer than broad, convex, in medial contact along a straight suture, the front edges forming a V-shape that contacts and frames the ascending process of the premaxilla, although the posterodorsal edge of the latter is far less angled; the lateral edges of nasals are curved downwards; posteroventral process of nasal contacts anteroventral process of frontal, ventral tip of frontal, directly above and medial to the contact zone of septomaxilla and frontal; vertical lamina of nasals laterally contacting medial edge of septomaxillae; the right nasal has a foramen in posteromedial region of the dorsal lamina.

The paired septomaxillae are separated by the vertical lamina of the nasals; each with a broad ascending conchal process, freely extending laterally beyond lateral margin of nasal in dorsal view, but not reaching the height of the lateral nasal edges; anteromedial process of septomaxilla is about one fifth the length of the septomaxilla, slightly curved and anterolaterally oriented, each reaching over about half the depth of the premaxilla and extending laterally to the lateral notches of the ascending process of the premaxilla, anterior tip of the process visible in dorsal view; posteromedial process is very long and thin, makes up about half the length of the entire septomaxilla, medially contacting vertical lamina of nasal, rounded posterior tip contacting anteroventral tip of frontal; the septomaxillary body is a complex structure made of very thin bone material with a rounded indentation in posterior view; the posterior region of the septomaxillary body and the ventral surface of the anterior half of the posteromedial process of the septomaxilla contact the anterior and anterodorsal region of the vomer.

The paired vomers are complex structures, about 1.7 times longer than broad, approaching, but not contacting each other medially, and with the anterior and posterior regions diverging; anteriorly and anterodorsally contacting septomaxilla, laterally approaching but not contacting anteromedial region of palatine; bifurcate vertical posteromedial laminae, diverging dorsally and ventrally, framing but not contacting choanal process of palatine anteriorly.

The paired prefrontals are 1.8 times longer than broad, widely separated, obliquely oriented, forming anterior margin of orbits;

the anterior margin is irregular; the posterior margin is slightly concave; in dorsal view, the central region is the narrowest, while the anteroventral region is expanded and the posterodorsal region is even more expanded; the posterodorsal edge contacts the anterolateral edge of the frontal along a slightly curved suture; the ventral edge contacts dorsal surface of maxilla lateroventrally and the maxillary process of palatine medioventrally; in rear view, a large lacrimal foramen is visible in ventromedial region.

The paired frontals are about twice as long as broad, slightly broader than nasals, slightly convex, in contact medially with a straight suture, together they are somewhat circular in dorsal view with undulated lateral margins; only a very short part of the lateral margin, directly posterior to the region of greatest width of the frontal participates in the formation of the dorsal margin of orbit; anterolateral edges of frontals forming an oblique, slightly curved suture with prefrontals; loose, curved suture between frontals and parietal, with long anterolateral processes of the parietal extending along the lateral edges of the frontals and almost reaching the contact zone with the prefrontals, excluding major parts of the frontals from the orbit; anteroventrally the frontal contacts the nasal and directly lateral and slightly ventral to this contact zone is a bulge whose anterior surface contacts the posterior end of the posteromedial process of the septomaxilla; laterally each frontal has a ventromedially oriented, slightly concave lamina along most of its length; anteromedially it has a vertical lamina along the first fifth of the bone, which is ventrally expanded and fused to the lateral lamina, forming a short tubular structure in the anterior region of each frontal; posterior to the tubular structure, the lateral lamina of both frontals are greatly separated, although they approach each other in the posterior region; the vertical laminae are in medial contact along most of their length, but are slightly separated in the ventral region, and contact again at the ventral apex, forming a small foramen between them; posterior to the ventral contact zone of the vertical lamina of the frontals is a facet, in which the anterior tip of the anterodorsal process of the parabasisphenoid intervenes, being the only contact region with the parabasisphenoid.

The single parietal is elongate, almost twice as long as broad, with long and robust anterolateral processes framing lateral borders of frontals and forming posterior and most of dorsal margin of orbit; in dorsal view, the parietal almost completely covers the pterygoids, of which only a small anterolateral portion is visible; anteriorly is a short medial groove, about 15% the length of the median region; a ridge extends dorsally on both sides from the anterolateral process in posteromedial direction, almost reaching the suture with the supraoccipital, the ridges approach each other, but remain distinctly separated; lateral to the dorsal ridges, the parietal slopes downwards with a convex surface to meet ventrally the posterior half of the parasphenoid rostrum and most of the basisphenoid portion of the parabasisphenoid; posterolaterally the parietal contacts the dorsal and anterior margins of the prootics and forms the anterior limit of the foramen for the maxillary branch of the trigeminal nerve at the lateral suture with the prootic; the posterodorsal region of the parietal is medially notched, forming a wavy suture with the supraoccipital. Postorbitals absent.

The single supraoccipital is ovoid, 1.7 times broader than long, slightly concave, anterior region is slightly elevated; anteriorly it contacts the parietal, anterolaterally the prootics, and posteriorly the exoccipitals; it is distinctly separated from the supratemporals; laterally the supraoccipital extends downwards (internal) to contribute to the dorsomedial walls of the otic capsules.

The paired exoccipitals are irregularly shaped, and slightly separated from each other with a straight median suture; each with an oblique, dorsolateral ridge parallel to the inner margin of supratemporals; anterodorsally each exoccipital contacts the supraoccipital with a curved suture, anterolaterally the prootic, ventrally the basioccipital and dorsolaterally the supratemporals; the fenestra ovalis is situated at the suture between prootic and exoccipital, and the exoccipital forms the posterior margin of the fenestra; posterior to the fenestra ovalis halfway to the foramen magnum is another relatively large foramen; several additional small foramina pierce the lateral and medial laminae of each exoccipital; posteroventrally, the occipital condyles approach each other, but remain separated through the posterior process of the basioccipital; the exoccipital contributes to the formation of the posteroventral, posteromedial and posterolateral wall of the otic capsule; posteriorly the exoccipitals form the dorsal, lateral, and lateroventral border of the foramen magnum.

The paired prootics are ovoid in lateral view, 1.2 times higher than long; each prootic contacts the parietal anteriorly and anterodorsally, the supraoccipital posterodorsally, the exoccipital posteriorly, the parabasisphenoid complex anteroventrally, the basioccipital posteroventrally, and the anterior part of the supratemporal dorsally; at the suture with the parietal it forms the posterior border of the foramen for the maxillary branch of the trigeminal nerve and at the suture with the exoccipital it forms the anterior margin of the fenestra ovalis; the foramen for the mandibular branch of the trigeminal nerve is posterolaterally oriented and situated slightly posterior to and slightly below the central part of the prootic in lateral view; between the trigeminal nerve foramina is a small foramen, and in the ventral region of the prootic, close to the suture with the parabasisphenoid is another, larger ovoid foramen; in dorsal view, the prootic bears a depression in the posterior region in which the anterior tip of the supratemporal rests; the prootic contributes to the formation of the anteroventral, anteromedial and anterolateral wall of the otic capsule; a few small foramina pierce the medial laminae of each exoccipital.

The unpaired parasphenoid and basisphenoid are fused to form the parabasisphenoid, which is further fused with the basioccipital, forming a convex, elongate structure, three times longer than broad, that occupies most of the skull floor; the basisphenoid and basioccipital portions are each roughly rounded, and the parasphenoid rostrum is lanceolate with a pointed anterior tip; the anterior tip of the parasphenoid rostrum bears a dorsally oriented process, which contacts the lower part of the frontals in anteromedial region; the anterior tip of the parasphenoid rostrum is separated from the choanal process of the palatine, the posterior ending of the vomers, nasals, and septomaxillae; dorsolaterally the parabasisphenoid–basioccipital complex contacts the parietal, the prootics posterior to it, and the exoccipitals in the posterior region; laterally, on each side where the parasphenoid rostrum meets the basisphenoid part of the bone, is a small anteriorly oriented foramen; where the parabasisphenoid is fused with the basioccipital there are several small foramina; two further, larger foramina are located in the posterior part of the basisphenoid portion, each at the lateral edge of the bone close to the suture with the prootics; posteriorly the square posterior process of the basioccipital portion forms the ventral border of the foramen magnum; at the widest part of the basioccipital portion, approximately at the beginning of the posterior half of the basioccipital, is a short, blunt, posteriorly pointing projection on each side of the outer lateral edges; a small foramen is present medially in the posterior region of the basioccipital portion, at about the region where the posterior process begins; in dorsal view the parabasisphenoid–basioccipital complex bears two round cavities separated by a ridge along the former suture of parabasisphenoid and basioccipital.

The palatomaxillary arch is composed of the maxillae, ectopterygoids, palatines, and pterygoids. The maxillae are elongate and robust, account for a little more than one quarter of the length of

the skull, and are almost four times as long as high, extending from the level of lateral processes of premaxilla to about central region of orbit, forming the anterior lower margin of orbit laterally; the maxilla is approximately triangular in lateral view, ignoring the teeth, with the highest point slightly anterior to the middle of the bone; slightly arched towards the premaxilla anteriorly; the ventral surface of the maxilla bears four tooth loci, with curved, and rear facing anterior teeth, slightly increasing in size posteriorly, followed posteriorly, after a distinct interspace, by a pair of large deeply grooved fangs, situated below the eye; the posterior end of the maxilla is approximately rectangular and without a tooth-like spur; of the cranial bones, the maxilla contacts only the prefrontal on its dorsal surface directly behind the highest point and anterior to the maxillary interspace; the palatine process is very short, approaching but not contacting the maxillary process of the palatine; an ectopterygoid process is not evident.

The ectopterygoids are forked, deeply bifurcated anteriorly, with a slightly longer medial process and a slightly shorter lateral process; in dorsal view of the skull, they are not covered by any other bone and are completely visible; the two anterior processes are directed anterolaterally and frame the posterior end of the maxilla laterally and medially without contacting it, forming a rather large maxilo-ectopterygoid fenestra; a rod-shaped posterior process medially meets the anterolateral portion of the pterygoid and has a slight narrowing in the contact zone.

The pterygoids are elongate, about 6.5 times longer than broad, corresponding to slightly more than half the length of the skull; in dorsal view of the skull, only the anterolateral region is visible and not covered by the parietal; ventral surface bears four tooth loci; teeth are subequal, small compared to maxillary teeth, slightly curved, rear facing; the anterior tip of the pterygoid does not protrude beyond the articulation with the ectopterygoid and dorsally overlaps only marginally the posterior edentulous tip of the palatine without touching it; in the anterior region to the level of the fourth tooth, which also corresponds to the contact zone with the ectopterygoid, the pterygoid is approximately rectangular, posteriorly it widens abruptly because of a lateral edge, which curves dorsally; in ventral view, the lateral border of the pterygoid is slightly curved posterolaterally; the medial borders of the pterygoids are approximately parallel in the anterior two thirds, with the smallest distance between them shortly after the tooth line; the medial border of the last third of the bone gradually tapers posterolaterally, greatest distance between the pterygoids is at their posterior tips; the posterior end of the pterygoid approaches medially the ventromedial process of the quadrate without touching it; in dorsal view the surface of the pterygoids is concave.

The palatines are elongated, more than five times as long as wide, excluding the choanal and maxillary process, correspond to 27% of the length of the skull, and represent the shortest of all toothed bones; although their medial edges are slightly curved, the palatines are approximately parallel; the ventral surface has five tooth loci; the teeth are solid, subequal, curved, and rear facing; of the cranial bones the palatine contacts only the medioventral region of the prefrontal on the dorsal surface of its maxillary process; the anterior portion of palatine approaches the ventrolateral part of vomer dorsally; dorsomedially, a long, thin choanal process rises and curves downwards in a semicircle, approaching but not contacting its counterpart medially; the short, stout, almost triangular maxillary process is situated on the lateral surface of palatine at the level of the second tooth, directed anterolaterally, approaching the palatine process of maxilla; the posterior part of the palatine behind the last tooth is bifurcated, with a slightly shorter and thinner ventrolateral branch and a slightly longer and broader dorsomedial branch, both tapering towards the posterior end, but ending bluntly and approaching the anterior part of the pterygoid, without contacting it.

The suspensorium is composed of the supratemporals and the quadrates. Each mandible is composed of the dentary, splenial, angular, and compound bone. The supratemporals are laminar, elongate, more than five times longer than wide and twisted in their posterior half; they are slightly oblique and diverge slightly posteriorly; in dorsal view, slightly less than the anterior half of each supratemporal overlaps and firmly contacts the posterior part of the prootic and the anterolateral part of the exoccipital over well-defined facets, the prootic is contacted only by the anterior tip of the supratemporal, while the contact surface with the exoccipital is more than twice as large; the supratemporals are distinctly separated from the parietal; the posterior part, except the proximal end, articulates laterally with the quadrate; the posterior end is free and protrudes posteriorly beyond the quadrate as well as the posterior end of the exoccipital and is thus the most posteriorly protruding bone of the skull roof.

The quadrates are flattened and broad dorsally, tapering dorsoventrally in lateral view, but gradually increasing in width in posterior view; they are oriented oblique, from anterodorsally to posteroventrally; the posterodorsal part loosely contacts the posterolateral region of the supratemporal medially; the medial part has a short process, which corresponds to the contact region with the columella auris, but the columella auris is barely visible; the ventral part is bifurcated, with the medial branch longer than the lateral branch and both together spanning the glenoid cavity of the retroarticular process of mandible; the quadrate does not exceed the posterior limit of the skull roof.

The dentaries are short, making up less than half the length of the mandible, and are slightly curved anteromedially; the dorsal surface bears 7–8 tooth loci; the teeth are subequal, curved and rear facing; the lateral face is slightly convex with a mental foramen located at about level of 3rd–4th tooth, slightly anterior to mid-region of dental tooth line; at about level of 7th tooth, the dentary branches into a shorter dorsal process, which overlays the anterior part of compound bone, and a longer lanceolate ventral process, which contacts the splenial and approaches the anterior part of the angular, and runs with its dorsal surface parallel and close along the anterior part of the medioventral region of the compound bone without touching it; dorsal process is posteriorly bifurcated with two branches of about the same length; the posterior part of the dorsal process seems to be slightly fractured in both mandibles.

The splenials are elongate, triangular, tapered anteriorly, almost four times longer than high, and represent the smallest of the mandibular bones, making up about one fifth of the mandibular length; the anterior mylohyoid foramen is in the dorsal region at about the beginning of the fourth quarter; the posterior edge of the splenial contacts the anterior region of the angular.

The angulars are elongate, triangular, tapered posteriorly, almost 4.4 times longer than high, and represent the second smallest of the mandibular bones, making up almost one third of the mandibular length; each angular contacts the splenial anteriorly and the compound bone laterally; the anterodorsal process approaches but does not contact the medial process of the dentary; the posterior mylohyoid foramen is on the lateral surface in anterior region of the bone.

The compound bones are elongate, seven times longer than high, and represent the largest of the mandibular bones, making up about 70% the length of the mandible; the prearticular crest is slightly higher than the surangular crest and thus visible in lateral view, the latter is not visible in medial view; in lateral view, the compound bone tapers anteriorly, loosely fitting between the dorsal and ventral processes of the dentary; at about the level where the posterior tip of the ventral process of the dentary ends is

an anterodorsally oriented foramen on the lateral surface of the bone; the retroarticular process is moderately long, it is slightly medially directed, extends beyond the posterior end of the exoccipitals and supratemporals, and marks the posterior limit of the skull.

3.2.12. Osteological comparisons

The skull of *Apostolepis assimilis* differs from *A. sanctaeritae* (Entiauspe-Neto et al., 2020, characters in parentheses) in having distinctly longer lateral processes of the premaxilla that are visible in dorsal view (short and not visible), sharply pointed posterior processes of the premaxilla (broad and blunt), parietal ridges approach each other, but remain distinctly separated (ridges merge in the posterior fifth of the parietal), parabasisphenoid and basioccipital bones fused (not fused), symmetrical bulges on the basioccipital absent (present), the anterior end of the supratemporal overlaps only the posterior part of the prootic and the posterior end protrudes posteriorly beyond the posterior end of the exoccipital and is thus the most posteriorly protruding bone of the skull roof (anterior end overlaying posterior half of prootic and posterior end not reaching posterior end of exoccipital), and by having a longer retroaticular process of the compound bone (short).

It differs from *A. cearensis* (Ferrarezzi et al., 2005, characters in parentheses) by having 4 pterygoid teeth (2), a prearticular crest of the compound bone that is higher than the surangular crest (same height as surangular crest), a U-shaped fronto-parietal suture in dorsal view without parietal indentation between frontals (W-shaped suture, with an antero-median parietal indentation), and nasal and prefrontal not in contact (in contact dorsally). Fig. 3.

4. Discussion

Based on our careful revision of available *nomina* and synonymy, the number of *Apostolepis* species is reduced to 34. The case of *A. tertulianobeui*, a synonym described upon a single specimen, has been repeated extensively in the taxonomic history of *Apostolepis* (see Entiauspe-Neto et al., 2019, 2020a, b). In the absence of comprehensive molecular data for the genus, our findings suggest that thorough revisions of morphological variation should assist in reevaluating the taxonomic status of poorly known taxa, and that further redescriptions and variation assessments should be made in order to increase the taxonomic stability in *Apostolepis*. The integration of multiple data sets (osteology, ecology, external morphology, osteology, hemipenial morphology) is also useful for delimiting species limits in *Apostolepis* species, where past diagnoses relied largely on subjective characters of external morphology.

Apostolepis assimilis seems to be a rare case in the genus, being well represented in collections. This species also seems to tolerate human disturbance, occurring in densely populated areas, as seen by the large series of individuals from São Paulo municipality, São Paulo, Brazil. The potential distribution for the species suggests a suitable area in eastern Bolivia, where the species has not been recorded yet. Although described more than 150 years ago, there

Table 2
Variation of the red *Apostolepis* species from the Cerrado. (SVL = snout-vent length; TL = tail length; ♂ = male; ♀ = female).

	A. assimilis	*A. cearensis*	*A. sanctaeritae*	*A. albicollaris*	*A. flavotorquata*
Head	Black	Black	Black	Black	Blackish brown
Light snout spot	Present; undivided, white.	Present; large, orange.	Present; large, orange.	Present; small, divided, white.	Present or absent; small, divided, white.
Supralabial blotch	Large, single, over 3rd to 5th supralabials	Small, single, over 3rd supralabials	Medium, single, over 3rd and 4th supralabials	Large, single, over 1st to 5th supralabials	Medium, two, largest over 3rd to 5th supralabials
Light nuchal collar	Present, large (usually up to four rows)	Present, large (usually up to five rows)	Present, two, large (usually up to five rows in first, three in second)	Present, large (usually up to four rows)	Present, small (usually up to two rows)
Black nuchal collar	Present, medium (usually up to three rows)	Present, medium (usually up to five rows)	Present, large (usually up to seven rows)	Present, medium (usually up to three rows)	Present, small (usually up to two rows)
Gular color	Immaculate cream	Immaculate cream or black	Immaculate cream or black	Immaculate cream or black	Immaculate cream
Dorsal background color	Orange or red	Orange	Orange	Red	Red or orange
Dorsal stripes	Absent	Absent	Absent	Absent	Absent or three
Ventral color	Immaculate cream or orange	Immaculate cream or orange	Immaculate cream or orange	Immaculate cream or black	Yellow
Tail black blotch	Present in dorsal and ventral view	Present in dorsal and ventral view	Present in dorsal and ventral view	Present in dorsal and ventral view	Present in dorsal and ventral view
Terminal spine	Black	Black	Black	Black or bicolor	Black or bicolor
Ventrals	225–260 (n = 21) ♂; 243–268 (n = 22) ♀	210–237 (n = 35) ♂; 235–242 (n = 29) ♀	219–240 (n = 12) ♂; 221–253 (n = 8) ♀	196–208 (n = 13) ♂; 206–230 (n = 10) ♀	245–268 (n = 4) ♂; 229–250 (n = 5) ♀
Subcaudals	26–36 (n = 19) ♂; 24–31 (n = 19) ♀	26–30 (n = 34) ♂; 21–31 (n = 25) ♀	32–36 (n = 8) ♂; 26–32 (n = 8) ♀	24–30 (n = 12) ♂; 28–33 (n = 10) ♀	31–40 (n = 4) ♂; 26–33 (n = 5) ♀
Supralabials	Six (rarely five or seven)	Six	Six	Six (rarely four, five, or seven)	Six
Infralabials	Six or seven	Six (rarely seven)	Seven	Six or seven (rarely eight)	Seven
Preocular-nasal contact	Absent	Absent	Absent	Present	Variable
Tail tip	Rounded	Slightly pointed	Pointed	Rounded	Rounded
Hemipenis	Slightly bilobed, almost simple and noncapitate, semicalyculate; body covered by moderately sized hooked spines on sulcate side	Unilobed, noncapitate, semicalyculate; body covered by large hooked spines on sulcate side	Slightly bilobed, almost simple and noncapitate, semicalyculate; body covered by moderately sized hooked spines on sulcate side	–	Unilobed, simple, noncapitate, calyculate; spinules restricted to proximal area, enlarged spines absent, asulcate surface calyculate

was no available information for its hemipenial morphology or osteology prior to this study.

The systematics of red *Apostolepis* species from the Cerrado needs to be formally evaluated. Although very similar in external morphology, *A. flavotorquata* and *A. assimilis* are strikingly different in hemipenial morphology (Table 2). The condition of a long, unilobed, simple, noncapitate, and calyculate hemipenis, present in *A. flavotorquata*, is also shared by *Apostolepis nigrolineata* and *Apostolepis thalesdelemai*, striped species from the Amazon and Caatinga Moist Forests respectively (Entiauspe-Neto et al., 2020a). According to McDowell (1986) "The occipital condyle of *Apostolepis* is unusual in having the exoccipital components brought together on its dorsal surface, rather than being separated by the basioccipital". However, this observation could not be confirmed in our analysis as the occipital condyles in the specimen of *A. assimilis* herein examined approach each other, but remain separated through the posterior process of the basioccipital.Boulenger, 1903, Guedes et al., 2018b (IZN, 1999), (lema, 2004) (Lema, 2016), (Peters, 1880).

Several gaps remain to be explored – natural history of *A. assimilis* is still poorly known, with little or no available information on its activity patterns, food habits, and reproduction. We argue that a large and integrative collaboration is warranted to increase the taxonomic stability and to provide a comprehensive systematic hypothesis for *Apostolepis*, with thorough genetic sampling; authors should also refrain from adopting unpublished taxonomic literature, as this can increase the already large taxonomic instability in the group.

Declaration of competing interest

The authors declare that they have no known competing financial interests or personal relationships that could have appeared to influence the work reported in this paper.

Acknowledgements

We are thankful to Editor A. Kupfer, R. C. Jadin and P. Cacciali, who provided a critical review and corrections to our manuscript. We thank W. S. Azevedo for helping us in the preparation of the plates. P. R. Møller (ZMUC), P. Passos (MNRJ), and R. B. Oliveira (MCN) kindly provided photos and data of specimens under their care. We also thank A. Martínez, A. D. Abegg (MZUSP), R. B. Oliveira (MCN), G. Horta, C. Cintra, M. A. Freitas (ICMBio), L. J. Vitt (OU), and W. Wüster (Bangor University) for contributing with photographs. OME-N thanks CNPq for a PIBIC grant (136628/2016-8). TBG thanks Universidade Estadual do Maranhão (Senior Researcher fellowship). DL thanks Conselho Nacional de Desenvolvimento Científico e Técnológico (CNPq) for the Research Productivity Fellowship (#310651/2017-4).

Appendix A. Supplementary data

Supplementary data to this article can be found online at https://doi.org/10.1016/j.jcz.2021.01.004.

Appendix I. Material examined

Countries are in bold capitals, states in capitals, municipalities and localities in plain text. Coordinates are given in SIRGAS2000.

***Apostolepis* aff. *niceforoi* (*n* = 1). BRAZIL:** RORAIMA: Caracara, Vila de Caicubi, Rio Jufari (MZUSP 19625).

***Apostolepis albicollaris* (n = 17). BRAZIL:** DISTRITO FEDERAL: Brasília (MCP 8354, 8355, 8436, 9188); GOIÁS: Goiânia (MCP 14638), Minaçu (MCP 8565, 15216, 15217, 15218, 15220, 15221, 15222, 15223, 15224, 15225, 15226, 15227); MINAS GERAIS: Monte Alegre (MCP 9191).

***Apostolepis arenaria* (*n* = 5). BRAZIL**: BAHIA: Alagoado (MZUSP 10027, 10028, 10029, 10030, 10289).

***Apostolepis assimilis* (*n* = 144). BRAZIL:** BAHIA: Barreiras (UMMZ 20411); DISTRITO FEDERAL: Brasília (CHUNB 24456, 24474, IBSP 20566, 28734, USNM 148790); GOIÁS: Ilha do Bananal, Santa Isabel (IBSP 12324); Jataí (MZUSP 3783); Mineiros (IBSP 55495); Rio Verde (IBSP 10326, 12945, MZUSP 3194), Uruaçu, Cana Brava (IBSP 9154); MINAS GERAIS: Cabo Verde (IBSP 29448); Cambuí (IBSP 44222), Capão dos Porcos, Mariana (ZMUC 63806, holotype of *Apostolepis assimilis*), Caxambu (IBSP 816), Conceição dos Ouros (IBSP 33206), Entre Rios de Minas (FUNED 691), Gonçalves (IBSP 49666), Ibirité (FUNED 603), Itajubá (IBSP 9115, 9407, 9592), Itamonte (IBSP 22405), Itatiaiaçu (FUNED 510), Jaíba (FUNED 1465), Maria da Fé (IBSP 5597), Moéda (FUNED 02), Nova Lima (FUNED 550), Ouro Fino (IBSP 34306), Munhoz (IBSP 66376), Passa Quatro (IBSP 3264, 3274, 34306), Poços de Caldas (IBSP 45737, 23985, 14256), Pouso Alegre (IBSP 42162, 44597, 49942), Santa Rosa da Serra (IBSP 46088), Serra do Cipó (MZUSP 7595), Uberabinha (IBSP 888) Uberlândia (IBSP 3841, 3845, 6388, 3841), Vespasiano (FUNED 04); MATO GROSSO DO SUL: Amambaí (IBSP 41163), Campo Grande (IBSP 41163, 42978, 57222, MHNCI 6719, MZUSP 10155) Nova Andradina (IBSP 27489, 27489), Paranaíba (IBSP 45615), Ponta Porã (IBSP 44065); MATO GROSSO: Buriti (IBSP 5346), Cuiabá (MNRJ 2031); PARANÁ: Londrina (IBSP 37462, 40008); SANTA CATARINA: Florianópolis (ZFMK 102210, previously BGSS5344, locality probably in error); SÃO PAULO: Araçariguama (IBSP 83132), Barueri (IBSP 23206), Bauru (MHNCI 4790), Cabreuva (IBSP 26565), Caieiras (IBSP 40320), Caixa d'Água (IBSP 6659), Carapicuiba (IBSP 87769, 82260), Cajamar (IBSP 30408, 87083, 3186), Campo Largo (IBSP 4498), Campo Limpo (IBSP 6532), Campos do Jordão (IBSP 26796, UMMZ 204112), Carapicuíba (IBSP 72970), Cotia (IBSP 24588), Ibiúna (IBSP 32672, 79312, 78900), Itapevi (IBSP 30436, 86908, 79489), Itatiba (IBSP 5703), Itu (IBSP 4180, 6606, 82230, MHNCI 6969, MZUSP 4180, 6606), Jaguara (IBSP 70356), Jandira (IBSP 31694, 40493), Jarinu (IBSP 30019), Jundiaí (IBSP 16688), Mairinque (IBSP 41065, 89049), Osasco (IBSP 23889, 40480, 6141, 62362, 78442, MCP 64), Pirituba (IBSP 70351, 78948), Rio Grande (IBSP 40008), Santana de Parnaíba (IBSP 61761, 81066), São Caetano do Sul (IBSP 81238), São Paulo (IBSP 318, 348, 6401, 6558, 8040, 8945, 21993, 22221, 24180, 24548, 24873, 27598, 30153, 30586, 31716, 32441, 33316, 84949, 78948), São Roque (IBSP 23548, 78641, 79658, MHNCI 4495, 6970), Sorocaba (IBSP 15760, 40008).

***Apostolepis cearensis* (*n* = 141). BRAZIL**: ALAGOAS: Piranhas (CHUFS 3217, 3365, MUFAL 1315); BAHIA: Brumado (IBSP 33651, 33685), Camaçari (MZUEFS 371), Capim Grosso (MZUEFS 294), Feira de Santana (MZUEFS 12, 19, 70, 71, 74, 86, 130, 162, 166, 203, 277, 310, 315, 429, 434, 463, 464, 505, 515, 615, 624, 637, 669, 672, 689, 771, 804, 836, 841, 895, 927, 1007, 1040, 1053, 1067, 1069, 1070, 1071, 1077, 1080, 1110, 1146, 1157, 1158, 1195, 1196, 1208, 1209, 1210, 1236, 1240, 1241, 1244, 1260, 1302, 1310, 1313, 1369, 1377, 1405, 1445, 1446, 1477, 1478, 1479, 1499, 1539, 1559, 1570, 1587, 1604, 1611, 1622, 1629, 1645, 1673, 1674), Poções (MZUFBA 1595, 1796, 1805, 1813, 1826, 1827), São Gonçalo dos Campos (MZUEFS 73, 825), Jaguarari (IBSP 26203); Tanque do Aragão, Central (MNRJ 6523); CEARÁ: Aquifaz (CHUFC 1185), Beberibe (CHUFC 1628), Cratéus (CHUFC 2238), Crato (IBSP 20385), Fortaleza (CHUFC 208, 826, 1240, 1242, 1243, 1524, 1525, 1526, 1527, 1528, 1529, 1531, 1539, 1620, 1621, 1622, 1623, 1623, 1624, 1625, 1626, 1627, 1629, 2001, 2236, 2287, 2243, 2633, IBSP 20020, 40262, 55318, 18219, 18220), Icó (IBSP 12106), Juazeiro do Norte (IBSP 20164), Limoeiro do Norte (IBSP 12775), Maranguape (CHUFC 2235), Quixadá (CHUFC 1221), São Benedito (CHUFC 2114, 2147), Tianguá (IBSP 77109), Ubajara (IBSP 75855, 77101), Viçosa do Ceará (IBSP 77509); PARAÍBA:

Cabaceiras (MZUSP 9013), Campina Grande (IBSP 9050), Lagoa de Dentro (MNRJ 17055); PIAUÍ: Teresina (IBSP 49743), Redenção do Gurgeia (IBSP 80942).

***Apostolepis cerradoensis* (*n* = 1). BRAZIL**: Goiás: Minaçu (MCP 15219, holotype of *Apostolepis cerradoensis*).

***Apostolepis christineae* (*n* = 2). BOLIVIA**: SANTA CRUZ: Puerto Suarez, German Busch (BMNH 1907.10.31.62). **BRAZIL**: MATO GROSSO: Cáceres (MCP 12515, holotype of *Apostolepis christineae*).

***Apostolepis dorbignyi* (*n* = 1)**. "AMÉRIQUE MÉRIDIONALE": Unknown locality (MNHN 3664, holotype of *Apostolepis dorbignyi*).

***Apostolepis flavotorquata* (n = 10). BRAZIL:** GOIÁS: Minaçu (MCP 15142, 15143, 15144, 15145, 15146, 15147, 15148, 15149, 15150, 15151); MATO GROSSO: Jacaré, Alto Xingu (SMS 93352).

***Apostolepis gaboi* (*n* = 34). BRAZIL**: BAHIA: Ibiraba-Barra (MZUFBA 1673, 1674, 1675, 1676, 1677, 1678, 1679, 1680, 1681, 1682, 1683, 1684, 1685, 1686, 1687, 1688, 1689, 1690, 1691, 1692, 1693, 1694, 1695, 1696, 1697, 1698, 1699, 1700, 1701, 1702, 1702, 1704), Icatú-Barra (MZUEFS 981), Queimadas (MZUSP 10290).

***Apostolepis goiasensis* (*n* = 1)**. **BRAZIL**: MINAS GERAIS: Três Lagoas (CHFURG 1344).

***Apostolepis intermedia* (*n* = 2). PARAGUAY**: San Pedro: Laguna Blanca (MHNP 11533, 11636).

***Apostolepis kikoi* (*n* = 5). BRAZIL**: MATO GROSSO: APM Manso, Chapada dos Guimarães (MCP 12096, 14524, 14525, 11372, UFMT-R 1933).

***Apostolepis longicaudata* (*n* = 1). BRAZIL**: TOCANTINS: Estação Ecológica Serra Geral (MZUSP 14122).

***Apostolepis multicincta* (*n* = 3). BOLIVIA**: SANTA CRUZ: San Juan (ZFMK 66375, paratype of *Apostolepis multicincta*), Florida (ZFMK 75025, 75026).

***Apostolepis nelsonjorgei* (*n* = 2). BRAZIL**: GOIÁS: Campinaçú (MZUSP 20636). TOCANTINS: Estação Ecológica Serra Geral (MZUSP 17615).

***Apostolepis nigrolineata* (*n* = 217).** SOUTH AMERICA (ZMB 6447, holotype of *Apostolepis nigrolineata*). **BRAZIL** (BMNH 1946.1.9.82, holotype of *Apostolepis pymi*). MARANHÃO: Paruá, BR 316 (MPEG 10835, 13641, 14352). MARANHÃO/PARÁ: BR 316, km 74 (MPEG.1064, 1084, 3581, 8192, 10851). MATO GROSSO: Paranaita (MZUSP 22344). PARÁ: Acará (MPEG 10939). Ananindeua (MPEG 6943, 9459). Apeú (MPEG 586, 587, 696, 1174, 1476, 1479, 2657, 2666, 3331, 3332, 3334, 3335, 5718, 6916, 6919, MCP 11317). Augusto Correa (MPEG 3905, 3954, 5399, 6712, 6713, 6721, 6724, 6737, 8999, 9937, 10764, 12450, 13074). Baião (MPEG 1596, 1600–1605, 1891–1897, 2101, 2422, 2423, 2560, 2822, 2826, 2864–2866, 3386, 3387, 3389, 3390, 3448, 3949, 3950, 3951, 4086, 4094, 4801, 4802, 4807, 4808, 4811, 4813–4817, 4828, 4858, 8187). Belém (IBSP 3033, 3034, 54152; KU 127256, 127257, 140153, 140154, MPEG 12769, 12770, 12771). Benevides: Genipaula Road, Pratinha (MPEG 7570, 8399, 8615, 8631, 12575, 14285, 15476); Cachoeira do Piriá (MPEG 2174, 2970, 5160, 7821, 7827, 9546, 9558, 9818, 9829, 11486, 11488, 11933, 11937, 12882, 12883, 15060, 15063, 15863). Castanhal (MPEG 5878, 7163, 7173, 10912, 10913, 11794, 12693). Gurupá (MPEG 16324). Igarapé-Açu (MPEG 868, 869, 870, 871, 910, 912, 913, 924, 925). Inhangabi (MPEG 1464, 1568, 1571). Marabá (MPEG 17304). Ilha de Outeiro (MCP 10718). Ourém (MPEG 4224, 5004, 5005, 5012, 7016, 7019). Santa Bárbara do Pará (MPEG 1855, 2608, 3952). Santarém (MPEG 8011). Santarém Novo (MPEG 1841, 1977, 3251, 4154, 4796, 7081). Santo Antônio do Tauá (MPEG 1000, 1453, 1872, 1873, 1879, 2375, 2376, 2643, 3306, 3940, 3940, 4718, 4720, 4721, 4723, 4730, 6958, 7557). Serra dos Carajás (MZUFV 1071). Serra de Kukoinhokren (MZUSP 10684-85). Uruá (IBSP 7285, MZUSP 7287). Utinga (KU 128094). Viseu (MPEG 1735, 1787, 2292, 2293, 2323, 2349, 3142-43 3714, 3953, 4458, 5239, 5249, 5320, 5321, 5324, 5325, 5327, 5329, 6633, 7291, 7325, 7338, 7701, 8959, 10010, 10884, 10886, 10887, 11267, 11268, 13260, 15126, 15127, 17279). RONDÔNIA: Machadinho do Oeste (MZUSP 21888). Pontes e Lacerda (MPEG 2500).

***Apostolepis quinquelineata* (*n* = 4). GUYANA:** Georgetown (BMNH 89.9.30.12, holotype of *Apostolepis quinquelineata*). **BRAZIL:** AMAZONAS: Presidente Figueiredo (INPA-H 31440); RONDÔNIA: Porto Velho (UFRO-H 228, 229).

***Apostolepis nigroterminata* (*n* = 3). BRAZIL**: MATO GROSSO: Comodoro (MPEG 26500). Vila Bela da Santíssima Trindade (MZUSP 6408). **PERU:** Cayaria (BMNH 1946.1.9.77, holotype).

***Apostolepis quirogai* (*n* = 1)**. **BRAZIL**: RIO GRANDE DO SUL: Santo Ângelo, Campus URI (MCP 12185).

***Apostolepis sanctaeritae* (*n* = 11)**. **BRAZIL**: BAHIA: Unknown locality (MCP 8442), Cocos (IBSP 61525, CHUNB 51360, CHUNB 23715), Correntina (CHUNB 39079), Santa Rita, Ibipetuba (NMW 23452, holotype of *Apostolepis sanctaeritae*; MZUFBA 728, topotype); MATO GROSSO: Nova Xavantina (MCP 8002), Ribeirão Cascalheira (MCP 19481); MINAS GERAIS: Pirapora (MPEG 18347), TOCANTINS: Palmas (IBSP 65267, holotype of *Apostolepis ammodites*).

***Apostolepis tenuis* (*n* = 1). BOLIVIA**: SANTA CRUZ: Buena Vista (UMMZ 64436, holotype of *Apostolepis tenuis*).

***Apostolepis thalesdelemai* (*n* = 39). BRAZIL**: CEARÁ: Guaramiranga (CHUFC 1950, 2067, 2353, 2371); Ibiapina (CHUFC 2337, 2340, 2342, 2343, 2351, 2437); Maranguape (CHUFC 2102, 2208, 2212, 2213, 2218, 2339, 2347, IBSP 80734); Pacoti (CHUFC 2344, 2346, 2463, 2731, 2841); São Benedito (CHUFC 2338); Ubajara (CHUFC 1349, 2085, 2110, 2137, 2154, 2341, 2350, 2769, 2954, IBSP 80735, ZUEC 3384).

***Apostolepis vittata* (*n* = 4). BRAZIL**: MATO GROSSO: Chapada dos Guimarães (ANSP 11293, holotype of *Rhynchonyx ambiniger vittatus*; CHUNB 30656), Parque Nacional Chapada dos Guimarães (UFMT-R 12259), Rio da Casca (MCP 13283).

References

Amaral, A., 1922. Contribuição para o conhecimento dos ofídios do Brazil. In: Parte I Quatro novas espécies de serpentes brasileiras. Mem. Inst. Butantan, vol. 1, pp. 1–37, 1921.

Amaral, A., 1935. Estudos sobre ophídios neotropicos XXXIII. Novas espécies de ophídios da Colombia. Mem. Inst. Butantan (Sao Paulo) 9, 219–223.

Baumgartner, J., Wilson, P., Esperón-Rodríguez, M., 2017. rmaxent: tools for working with Maxent in R. R package version 0, 8, p. 3. https://github.com/johnbaums/rmaxent.

Bradie, J., Leung, B., 2017. A quantitative synthesis of the importance of variables used in MaxEnt species distribution models. J. Biogeogr. 44, 1344–1361. https://doi.org/10.1111/jbi.12894.

Braz, H.B., Kasperoviczus, K.N., Guedes, T.B., 2019. Reproductive biology of the fossorial snake *Apostolepis gaboi* (Elapomorphini): a Threatened and poorly known species from the Caatinga region. S. Am. J. Herpetol. 14, 37e47. https://doi.org/10.2994/SAJH-D-17-00116.1.

Borges-Nojosa, D.M., Lima, D.C., Bezerra, C.H., Harris, J.H., 2017. Two new species of *Apostolepis* Cope, 1862 (serpentes: Elapomorphini) from brejos de Altitude in northeastern Brazil. Rev. Nordest. de Zool. 10, 74–94, 2016.

Boulenger, G.A., 1896. Catalogue of Snakes in the British Museum, vol. 3. Taylor and Francis.

Boulenger, G.A., 1903. Descriptions of new snakes in the collection of the British Museum. Ann. Mag. Nat. Hist. 12, 350–354. https://doi.org/10.1080/00222930308678866.

Bullock, R.E., Tanner, W.W., 1966. A comparative osteological study of two species of Colubridae (*Pituophis* and *Thamnophis*). Brigham Young Univ. Sci. Bull. Biol. 8, 1–29.

Costa, H.C., Bérnils, R.S., 2015. *Apostolepis parassimilis* lema & renner, 2012 an objective synonym of *A. tertulianobeui* lema, 2004 (dipsadidae: Elapomorphini). Zootaxa 3957, 243–245. https://doi.org/10.11646/zootaxa.3957.2.10.

Cope, E.D., 1887. Synopsis of the batrachia and reptilia obtained by H. H. Smith in the province of Mato Grosso, Brazil. Proc. Am. Philos. 24, 44–60.

Cruz-da-Silva, R.C., de Freitas, M.A., Abegg, A.D., 2018. A remarkable specimen of the genus *Anilius* (Serpentes: aniliidae): rare colour aberration or a new species? Herpetol. Notes. 11, 161–165.

Cundall, D., Irish, F., 2008. The snake skull. In: Gans, C., Gaunt, A.S., Adler, K. (Eds.), The Skull of Lepidosauria, vol. 20. Society for the Study of Amphibian and Reptiles Press, Ithaca, pp. 349–692. Biology of Reptilia.

De Queiroz, K., 2007. Species concepts and species delimitation. Syst. Biol. 56, 879–886. https://doi.org/10.1080/10635150701701083.

Dowling, H.G., 1951. A proposed standard system of counting ventrals in snakes. Br. J. Herpetol. 1, 97–99.
Dowling, H.G., Savage, J.M., 1960. A guide to snake hemipenis: a survey of basic structure and systematic characteristics. Zoologica 45, 17–28.
Duméril, A.M.C., Bibron, G., Duméril, A.H.A., 1854. Erpétologie généralé ou histoire naturelle complète des reptiles. Tome septième. Deuxième partie, comprenant l'histoire des serpentes venimeux. Lib. Enc. Roret 781–1536.
Entiauspe-Neto, O.M., Lema, T., Beconi, H.E.C., 2014. *Apostolepis intermedia* Koslowsky, 1898 (serpentes: xenodontinae: Elapomorphini): first records for Paraguay. Check List. 10, 600–601. https://doi.org/10.15560/10.3.600.
Entiauspe-Neto, O.M., Sena, A., Tiutenko, A., Loebmann, D., 2019. Taxonomic status of *Apostolepis barrioi* lema, 1978, with comments on the taxonomic instability of *Apostolepis* Cope, 1862 (serpentes, dipsadidae). ZooKeys 841, 71–78. https://doi.org/10.3897/zookeys.841.33404.
Entiauspe-Neto, O.M., Guedes, T.B., Loebmann, D., Lema, T., 2020a. Taxonomic status of two simultaneously described *Apostolepis* Cope, 1862 species (dipsadidae: Elapomorphini) from Caatinga enclaves moist Forests, Brazil. J. Herpetol. 54, 225–234. https://doi.org/10.1670/19-053.
Entiauspe-Neto, O.M., Koch, C., Guedes, T.B., Tiutenko, A., 2020b. Revisiting the taxonomic status of *Apostolepis sanctaeritae*, a forgotten Neotropical dipsadid snake. Salamandra 56, 1–14.
Entiauspe-Neto, O.M., Tiutenko, A., 2020. On the taxonomic status of *Apostolepis roncadori* lema, 2016 and *Apostolepis vittata* (Cope, 1887) (serpentes: dipsadidae). Rev. Lat. Herpetol. In Press.
Feng, X., Park, D.S., Liang, Y., Pandey, R., Papeş, M., 2019. Collinearity in ecological niche modeling: confusions and challenges. Ecol. Evol. 9, 10365–10376. https://doi.org/10.1002/ece3.5555.
Fermiano, E.C., Silva-Alves, V.D., da Silva, O.D., Seba, M.D.F.R., Goebel, L.G.A., dos Santos-Filho, M., da Silva, D.J., 2020. New records of *Apostolepis kikoi* Santos et al., 2018 (Serpentes, Dipsadidae) in the state of Mato Grosso, Central-West Brazil. Check List. 16, 1049–1053. https://doi.org/10.15560/16.4.1049.
Ferrarezzi, H., 1993. Sistemática Filogenética de *Elapomorphus, Phalotris* e *Apostolepis* (Serpentes: Colubridae: Xenodontinae). Departamento de Zoologia, Instituto de Biociências, Universidade de São Paulo, São Paulo, p. 277. MSc. dissertation.
Ferrarezzi, H., Barbo, F.E., Albuquerque, C.E., 2005. Phylogenetic relationships of a new species of *Apostolepis* from Brazilian cerrado, with notes on the *assimilis* group (Serpentes: colubridae: Xenodontinae: Elapomorphini). Pap. Avulsos Zool. (Sao Paulo) 45, 215–229. https://doi.org/10.1590/S0031-10492005001600001.
Fick, S.E., Hijmans, R.J., 2017. Worldclim 2: new 1-km spatial resolution climate surfaces for global land areas. Int. J. Climatol. 37, 4302–4315. https://doi.org/10.1002/joc.5086.
França, D.P.F., Barbo, F.E., Silva-Júnior, N.J., Silva, H.L.R., Zaher, H., 2018. A new species of *Apostolepis* (serpentes, dipsadidae, Elapomorphini) from the cerrado of Central Brazil. Zootaxa 4521, 539–552. https://doi.org/10.11646/zootaxa.4521.4.3.
Giraudo, A., Scrocchi, G.J., 1998. A new species of *Apostolepis* (Serpentes: colubridae) and comments on the genus in Argentina. Herpetologica 54, 470–476.
Gomes, J.F., 1915. Contribuição para o conhecimento dos ophidios do Brasil. 1. Descrição de quatro espécies novas e um novo Gênero de opisthóglyphos. 2. Ophidios do Museu Rocha (Ceará). An. Paul. Med. Cir. 4, 121–129.
Guedes, T.B., Barbo, F.E., França, D.P.F., Zaher, H., 2018a. Morphological variation of the rare psammophilous species *Apostolepis gaboi* (Serpentes, Dipsadidae, Elapomorphini). Zootaxa 4418, 469–480. https://doi.org/10.11646/zootaxa.4418.5.4.
Guedes, T.B., Sawaya, R.J., Zizka, A., Laffan, S., Faurby, S., Pyron, R.A., Bérnils, R.S., Jansen, M., Passos, P., Prudente, A.L.C., Cisneros-Heredia, D.F., Braz, H.B., Nogueira, C.C., Antonelli, A., 2018b. Patterns, biases and prospects in the distribution and diversity of Neotropical snakes. Global Ecol. Biogeogr. 27, 14–21. https://doi.org/10.1111/geb.12679.
Harvey, M.B., 1999. Revision of Bolivian *Apostolepis* (squamata: colubridae). Copeia 388–409. https://doi.org/10.2307/1447485, 1999.
Harvey, M.B., Gonzales, L., Scrocchi, G.J., 2001. New species of *Apostolepis* (squamata: colubridae) from gran Chaco in southern Bolivia. Copeia 501–507. https://doi.org/10.1643/0045-8511(2001)001[0501:NSOASC]2.0.CO;2, 2001.
Hijmans, R.J., Phillips, S., Leathwick, J., Elith, J., Hijmans, M.R.J., 2017. Package 'dismo'. https://cran.r-project.org/web/packages/dismo/dismo.pdf.
Hijmans, R.J., Van Etten, J., Cheng, J., Mattiuzzi, M., Sumner, M., Greenberg, J.A., Hijmans, M.R.J., 2015. Package 'raster'. https://cran.r-project.org/web/packages/raster/raster.pdf.
ICZN, 1999. International Code of Zoological Nomenclature, fourth ed. International Trust for Zoological Nomenclature, London.
Jan, G., 1862. Enumerazione sistematico delle specie d'ofidi del gruppo Calamaridae. Arch. Zool. Anat. Fisiol. 2, 1–76.
Koslowsky, J., 1898. Ofidios de Matto-Grosso (Brazil). Rev. Mus. La Plata 8, 25–34.
Lamigueiro, O.P., Hijmans, R., Lamigueiro, M.O.P., 2019. Package 'rasterVis. '. https://cran.r-project.org/web/packages/rasterVis/rasterVis.pdf.
Lema, T., 2001. Fossorial snake genus *Apostolepis* from south America (serpentes: colubridae: elapomorphinae). Cuad. Herpetol. 15, 29–43.
Lema, T., 2004a. Nova espécie de *Apostolepis* do grupo *lineata* do sudoeste do Brasil (Serpentes, Elapomorphinae). Facena 18, 41–52.
Lema, T., 2003. Descrição de nova espécie de *Apostolepis* Cope do Cerrado do Brasil, pertencente ao grupo *dimidiata* (Serpentes, Elapomorphinae). Acta Biol. Leopoldensia 25, 123–131.
Lema, T., 2004b. Description of a new species of *Apostolepis* Cope, 1861 (serpentes, elapomorphinae) from Brazilian cerrado. Acta Biol. Leopoldensia 26, 155–160.
Lema, T., 2004c. Nova espécie de *Apostolepis* Cope do estado de Rondônia, brasil (serpentes, elapomorphinae). Comun. Mus. Cienc. Tecnol. Pucrs. Ser. Zool. 17, 81–89.
Lema, T., 2016. Description of new species of *Apostolepis* (serpentes: dipsadidae: xenodontinae: Elapomorphini) from Serra do roncador, Central Brazil. Cad. Pesqui. Sér. Biol. 28, 1–12.
Lema, T., Campbell, P., 2017. New species of *Apostolepis* (serpentes, dipsadinae, Elapomorphini) from Bolivia, from the *Apostolepis borellii* group. J. Zool. Sci. 5 (1), 19–28.
Lema, T., Renner, M.F., 2004. New species of *Apostolepis* from Alto Tocantins, Brazil, with comments on the striped pattern species (serpentes, elapomorphinae). Biociencias 12, 139–145.
Lema, T., Renner, M.F., 2006. A new species of *Apostolepis* with striped pattern from Mato Grosso, brasil (serpentes, elapomorphine). Ciênc. Mov. 8, 13–18.
Lema, T., Renner, M.F., 2007. Contribuição ao conhecimento de *Apostolepis ammodites* (Serpentes, Colubridae, Elapomorphinae). Biociencias 15, 126–142.
Lema, T., Renner, M.F., 2012. A new species of *Apostolepis* (Serpentes, Colubridae, Elapomorphini), belonging to *assimilis* group, found in Brazilian Cerrado. Rev. Ciênc. Mov. 13, 71–76.
Linnaeus, C., 1758. Systema Naturæ Per Regna Tria Naturæ, Secundum Classes, Ordines, Genera, Species, Cum Characteribus, Differentiis, Synonymis, Locis. Tomus I. Editio Decima, Reformata. Laurentii Salvii, Holmiæ.
McDowell, S.B., 1986. The architecture of the corner of the mouth of colubroid snakes. J. Herpetol. 20, 353–407. https://doi.org/10.2307/1564502.
Muscarella, R., Galante, P.J., Soley-Guardia, M., Boria, R.A., Kass, J.M., Uriarte, M., Anderson, R.P., 2016. Package "ENMeval: automated runs and evaluations of ecological niche models". https://cran.r-project.org/web/packages/ENMeval/index.html.
Naimi, B., 2015. usdm: uncertainty analysis for species distribution models. R package version 1.1–15. http://www.rdocu-mentation.org/packages/usdm.
Nogueira, C., Barbo, F.E., Ferrarezzi, H., 2012. Redescription of Apostolepis albicollaris lema, 2002, with a key for the species groups of the genus Apostolepis (serpentes: dipsadidae: Elapomorphini). S. Am. J. Herpetol. 7, 213–225. https://doi.org/10.2994/057.007.0303.
Nogueira, C.C., Argôlo, A.J., Arzamendia, V., Azevedo, J.A., Barbo, F.E., Bérnils, R.S., Bolocho, B.E., Borges-Martins, M., Brasil-Godinho, M., Braz, H., Buononato, M.A., Cisneros-Heredia, D.F., Colli, G.R.C., Costa, H.C., Franco, F.L., Giraudo, A., Gonzalez, R.C., Guedes, T., Hoogmoed, M.S., Marques, O.A.V., Montingelli, G.G., Passos, P., Prudente, A.L.C., Rivas, G.A., Sanchez, P.M., Serrano, F.C., Silva-Jr, N.J., Strüssmann, C., Vieira-Alencar, J.P.S., Zaher, H., Sawaya, R.J., Martins, M., 2019. Atlas of Brazilian snakes: verified point-locality maps to mitigate the Wallacean shortfall in a megadiverse snake fauna. S. Am. J. Herpetol. 14 https://doi.org/10.2994/SAJH-D-19-00120.1, 1-274.
O'Donnell, M.S., Ignizio, D.A., 2012. Bioclimatic predictors for supporting ecological applications in the conterminous United States. US Geol. Surv. Data Series 691, 10.
Peracca, M.G., 1904. Viaggio del Dr. A. Borelli nel Matto Grosso brasiliano e nel Paraguay, 1899. IX. Rettili ed amfibii. Boll. mus. zool. Torino 19, 1–15.
Prado, A., 1942. Notas ofiológicas. 14. Comentários acerca de algumas serpentes opistóglifas do gênero Apostolepis, com a descrição de uma nova espécie. Mem. Inst. Butantan (Sao Paulo) 16, 7–12.
Pesantes, O.S., 1994. A method for preparing the hemipenis of preserved snakes. J. Herpetol. 28, 93–95. https://doi.org/10.2307/1564686.
Peters, W.C.H., 1869. Über neue Gattungen und neue oder weniger bekannte Arten von Amphibien (Eremias, Dicrodon, Euprepes, Lygosoma, Typhlops, Eryx, Rhynconix, Elapomorphus, Achalinus, Coronella, Dromicus, Xenopholis, Anoplodipsas, Spilotes, Tropidonotus). Ber. Akad. Wiss, Berlin, pp. 432–447.
Peters, W.C.H., 1880. Eine Mittheilung über neue oder weniger bekannte Amphibien des Berliner Zoologischen Museums (*Leposoma dispar, Monopeltis* (*Phractogonus jugularis, Typhlops depressus, Leptocalamus drilineatus, Xenodon punctatus, Elapomorphus erythronotus, Hylomantis*)). Ber. Akad. Wiss. Berlin., pp. 217–224
Phillips, S.J., 2006. A brief tutorial on Maxent. AT&T Research. http://biodiversityinformatics.amnh.org/open_source/maxent/.
Radosavljevic, A., Anderson, R.P., 2014. Making better Maxent models of species distributions: complexity, overfitting and evaluation. J. Biogeogr. 41, 629–643. https://doi.org/10.1111/jbi.12227.
Reinhardt, J.T., 1861. Herpetologiske Middelelser. II. Beskrivelser af nogle nye til Calamariernes Familie henhörende Slänger. Vidensk. Meddel. Naturhist. Foren. Kjöbenhavn 2, 229–250, 1860.
Rodrigues, M.T., 1993. Herpetofauna das dunas interiores do Rio São Francisco: Bahia: Brasil. V. Duas novas espécies de *Apostolepis* (Ophidia, Colubridae). Mem. Inst. Butantan (Sao Paulo) 54, 53–59.
Ruthven, A.G., 1927. Description of an apparently new species of *Apostolepis* from Bolivia. Occas. Pap. Mus. Zool. Univ. Mich. 188, 1–2.
Sanderson, E.W., Jaiteh, M., Levy, M.A., Redford, K.H., Wannebo, A.V., Woolmer, G., 2002. The human footprint and the last of the wild: the human footprint is a global map of human influence on the land surface, which suggests that human beings are stewards of nature, whether we like it or not. Bioscience 52, 891–904. https://doi.org/10.1641/0006-3568(2002)052[0891:THFATL]2.0.CO;2.
Santos, F.M., Entiauspe-Neto, O.M., Araújo, J.S., de Souza, M.B., Lema, T., Strussmann, C., de Albuquerque, N.R., 2018. A new species of burrowing snake (Serpentes: dipsadidae: *Apostolepis*) from the state of Mato Grosso, Central-

West region of Brazil. Zool. 35, 1–10. https://doi.org/10.3897/zoologia.35.e26742.
Schlegel, H., 1837. In: Kips, J., Hz, J. (Eds.), Essai sur la physionomie des serpens. Partie Descriptive. van Stockum, La Haye.
Smith, P., Clay, R., 2015. Six new or important departmental herpetological records for Paraguay. Paraq. Nat. 3, 20–22.
Uetz, P., Hošek, J., 2020. The reptile database. Available from: http://www.reptile-database.org. (Accessed 11 September 2020).
Wickham, H., 2011. ggplot2. WIREs Comp Stat 3, 180–185.
Werner, F., 1924. Neue oder wenig bekannte Schlangen aus dem Naturhistorischen Staatsmuseum in Wien. I. Teil. Sitz. Ber. K. Akad. Wiss. 133, 29–56.
Zaher, H., 1999. Hemipenial morphology of the South American Xenodontine snakes, with a proposal for a monophyletic Xenodontinae and a reappraisal of colubroid hemipenes. Bull. Am. Mus. Nat. Hist. 240, 1–168.
Zaher, H., Prudente, A.L.C., 2003. Hemipenis of *siphlophis* (serpentes, xenodontinae) and techniques of hemipenial preparation in snakes: a response to dowling. Herpetol. Rev. 34, 302–307.
Zar, J.H., 1999. Biostatistical Analysis, 4th Edition. Prentice Hill.
Zurell, D., Franklin, J., König, C., Bouchet, P.J., Dormann, C.F., Elith, J., Fandos, G., Feng, X., Guillera-Arroita, G., Guisan, A., Lahoz-Monfort, J.J., Leitão, P.J., Park, D.S., Peterson, A.T., Rapacciuolo, G., Schmatz, D.R., Schröder, B., Serra-Diaz, J.M., Thuiller, W., Yates, K.L., Zimmermann, N.E., Merow, C., 2020. A standard protocol for reporting species distribution models. Ecography 43, 1261–1277. https://doi.org/10.1111/ecog.04960.